International Journal of Nanomedicine

Dovepress
open access to scientific and medical research

Open Access Full Text Article

ORIGINAL RESEARCH

Silver Nanoparticle-Induced Apoptosis in ARPE-19 Cells Is Inhibited by *Toxoplasma gondii* Pre-Infection Through Suppression of NOX4-Dependent ROS Generation

This article was published in the following Dove Press journal:
International Journal of Nanomedicine

Juan-Hua Quan[1,*]
Fei Fei Gao[2,*]
Hassan Ahmed Hassan Ahmed Ismail[3,*]
Jae-Min Yuk[2]
Guang-Ho Cha[2]
Jia-Qi Chu[4]
Young-Ha Lee[2]

[1]Department of Gastroenterology, The Affiliated Hospital of Guangdong Medical University, Zhanjiang 524-001, People's Republic of China; [2]Department of Infection Biology and Department of Medical Science, Chungnam National University College of Medicine, Daejeon 301-131, Korea; [3]Communicable and Non-Communicable Diseases Control Directorate, Federal Ministry of Health, Khartoum, Sudan; [4]Stem Cell Research and Cellular Therapy Center, Affiliated Hospital of Guangdong Medical University, Zhanjiang, Guangdong Province 524-001, People's Republic of China

*These authors contributed equally to this work

Correspondence: Young-Ha Lee
Department of Infection Biology and Department of Medical Science, Chungnam National University College of Medicine 6 Munhwa-Dong, Jung-Gu, Daejeon 35015, Korea
Tel +82-42-580-8273
Fax +82-42-583-8216
Email yhalee@cnu.ac.kr

Purpose: External and internal stimuli easily affect the retina. Studies have shown that cells infected with *Toxoplasma gondii* are resistant to multiple inducers of apoptosis. Nanoparticles (NPs) have been widely used in biomedical fields; however, little is known about cytotoxicity caused by NPs in the retina and the modulators that inhibit nanotoxicity.

Materials and Methods: ARPE-19 cells from human retinal pigment epithelium were treated with silver nanoparticles (AgNPs) alone or in combination with *T. gondii*. Then, the cellular toxicity, apoptosis, cell cycle analysis, autophagy, ROS generation, NOX4 expression, and MAPK/mTOR signaling pathways were investigated. To confirm the AgNP-induced cytotoxicity in ARPE-19 cells and its modulatory effects caused by *T. gondii* infection, the major experiments carried out in ARPE-19 cells were performed again using human foreskin fibroblast (HFF) cells and bone marrow-derived macrophages (BMDMs) from NOX4$^{-/-}$ mice.

Results: AgNPs dose-dependently induced cytotoxicity and cell death in ARPE-19 cells. Apoptosis, sub-G1 phase cell accumulation, autophagy, JNK phosphorylation, and mitochondrial apoptotic features, such as caspase-3 and PARP cleavages, mitochondrial membrane potential depolarization, and cytochrome c release into the cytosol were observed in AgNP-treated cells. AgNP treatment also increased the Bax, Bik, and Bim protein levels as well as NOX4-dependent ROS generation. However, *T. gondii*-infected ARPE-19 cells inhibited AgNP-induced apoptosis, JNK phosphorylation, sub-G1 phase cell accumulation, autophagy, NOX4-mediated ROS production, and mitochondrial apoptosis. Furthermore, mitochondrial apoptosis was found in AgNP-treated HFF cells and BMDMs, and AgNP-induced mitochondrial apoptosis inhibition via NOX4-dependent ROS suppression in *T. gondii* pre-infected HFF cells and BMDMs was also confirmed.

Conclusion: AgNPs induced mitochondrial apoptosis in human RPE cells combined with cell cycle dysregulation and autophagy; however, these effects were significantly inhibited by *T. gondii* pre-infection by suppression of NOX4-mediated ROS production, suggesting that *T. gondii* is a strong inhibitory modulator of nanotoxicity in in vitro models.

Keywords: silver nanoparticles, *Toxoplasma gondii*, mitochondrial apoptosis, human retinal pigment epithelium, reactive oxygen species, NADPH oxidase 4

Introduction

Nanoparticles (NPs) have been widely used in biomedical applications, such as therapeutics, biomedical device coating, detection and diagnosis platforms, drug-delivery carriers, and fluorescent labels. Silver nanoparticles (AgNPs) are among the most commonly used nanomaterials. They are used in the manufacture of many

submit your manuscript | www.dovepress.com
DovePress
http://doi.org/10.2147/IJN.S244785

consumer products and as a constituent element of catheters, implant surfaces, and for drug delivery in cancer and retinal therapies.[1,2] The physicochemical properties of AgNPs can be considered as dependent on different kinds of properties such as NP size, shape, concentration, agglomeration, or aggregation.[3] AgNPs easily penetrate across cell barriers, preferentially accumulate in specific organelles and cells, and show theranostic properties and the capacity for fine-tuning.[4,5] Numerous studies have shown that AgNPs induce cytotoxic responses, such as increased production of reactive oxygen species (ROS), apoptosis, DNA damage, and proinflammation at the molecular and cellular levels.[4,5] Regarding the AgNP-induced cytotoxicity, AgNPs induce size-dependent cytotoxicity, and cell viability decreases in a concentration-dependent manner.[4,5] And the strong oxidative activity of AgNPs releases silver ions, which have several negative effects on biological systems by inducing cytotoxicity, genotoxicity, immunological responses, and even cell death.[4–6] The cytotoxicity of AgNPs has been examined in several in vitro studies using human lung cell lines,[7] human liver cell lines,[8] and others. In animal eye tissues, AgNPs suppress the proliferation and migration of bovine retinal endothelial cells and exhibit an anti-angiogenic potential,[9] as well as induce significant neurotoxic effects in in vitro-cultured mouse retinal tissues.[10] However, it is crucial to understand the effects, possible toxicity, and health risks of AgNPs when they are applied in the human eye tissues.

Retinal pigment epithelium (RPE) is a vital cell layer and plays a role in upholding visual function situated between the choroid and photoreceptors of the eye. It forms a blood-retina barrier and is centrally involved in the pathogenesis of retinal diseases.[11] According to the previous studies related to NPs and retina, AgNPs inhibit the endothelial cell permeability of the blood-retina barrier through the Src kinase pathway.[12] Mulberry leaf extract mediated AgNPs and resveratrol coated gold NPs have been shown to ameliorate diabetic retinopathy in a rat model.[13,14] Similar to the above-mentioned studies, AgNPs have been applied in the ocular field either as the active component or as a carrier of a functional agent;[11–16] however, the literature on the evaluation of adverse effects on the ocular tissue after exposure of AgNPs is rare.

Toxoplasma gondii is an obligate intracellular protozoan parasite and is widely prevalent in animals and humans. *T. gondii* can actively invade and replicate in all nucleated cells, particularly in the brain and retina.[17] It has developed several strategies, such as resistance to oxidative stress and modulation of host cell survival and death to obtain lifelong parasite survival, to avoid destruction by internal and external stimuli.[17,18] Several studies have shown that cells infected with *T. gondii* are resistant to multiple inducers of apoptosis, including Fas-dependent and Fas-independent CTL-mediated cytotoxicity, IL-2 deprivation, irradiation, UV irradiation, the calcium ionophore beauvericin, and actinomycin D, staurosporine, exogenous cytochrome c and dATP.[19–23] *T. gondii* inhibits staurosporine- or exogenous cytochrome *c*/dATP-induced mitochondrial apoptosis by preventing the release of cytochrome *c* and phosphorylation of the pro-apoptotic Bad protein and inducing overproduction of the anti-apoptotic protein Bcl-2.[22,23] *T. gondii* can prolong its parasitism by modulating the host cellular defense system; however, little is known about the modulatory effect of *T. gondii* in AgNP-induced cytotoxicity in human hosts.

With the growing use of nanotechnology in the field of ophthalmology, RPE can receive various external and internal stimuli; however, no information regarding the nanotoxicity of human RPE cells has yet been reported. *T. gondii* has the ability to inhibit apoptosis in several murine and human host cells against a broad spectrum of proapoptotic stimuli;[17–23] however, the anti-apoptotic activity against NPs has not yet been investigated. Thus, to investigate the nanotoxicity of AgNPs and its mechanisms in human RPE ARPE-19 cells, as well as modulatory effect of *T. gondii* in AgNP-treated RPE, ARPE-19 cells were treated with AgNPs alone or in combination with *T. gondii*, and then, the cellular toxicity, apoptosis, cell cycle analysis, autophagy, ROS generation, NOX4 expression, and mitogen-activated protein kinase (MAPK) and mTOR signaling pathways were investigated. To confirm the AgNP-induced cytotoxicity in ARPE-19 cells and its modulatory effects caused by *T. gondii* infection, the major experiments carried out in ARPE-19 cells were performed again using human foreskin fibroblast (HFF) cells and bone marrow-derived macrophages (BMDMs) from $NOX4^{-/-}$ mice.

Materials and Methods

Silver Nanoparticles (AgNPs)

AgNPs were obtained from Nano Chemical Inc. (Silvergen™, Daejeon, South Korea). Characterization of AgNPs was previously reported.[24] In brief, primary particle size was measured using a transmission electron microscope (JEM-3020, 300 kV; JEOL, Tokyo, Japan) (Supplementary Figure 1). The particles have a spherical shape, and the mean particle size was determined as 6.0 ± 0.29 nm. The dynamic light scattering result showed that

the average hydrodynamic diameter of AgNPs was 24.7 ± 0.235 nm, and the zeta potential value of the nanoparticles was 88.67 ± 0.253 mV.

Reagents

Texas Red-X phalloidin, LIVE/DEAD Fixable Red Dead Cell Stain kit, CellROX deep red reagent and MitoSOX red mitochondrial superoxide indicator were purchased from ThermoFisher Scientific (Waltham, MA, USA). CytoTox 96 Non-Radioactive Cytotoxicity Assay was obtained from Promega (Madison,WI, USA). Cell cycle regulation antibody sampler kit II, anti-cleaved caspase-3, anti- poly(ADP-ribose) polymerase (PARP), anti-LC3B, Pro-Apoptosis Bcl-2 Family Antibody Sampler Kit, Pro-Survival Bcl-2 Family Antibody Sampler Kit, anti-Cytochrome c, anti-COX IV, anti-phospho-AKT (p-AKT), anti-AKT, anti-phospho-mTOR (p-mTOR), anti-mTOR, anti-phospho-p38 MAPK (p-p38), anti-p38 MAPK, anti-phospho-ERK1/2 (p-ERK1/2), anti-ERK1/2, anti-phospho-JNK (p-JNK), anti-JNK antibodies were purchased from Cell Signaling Technology Inc. (Danvers, MA, USA). Anti-NOX4 antibody was obtained from Abcam (Cambridge, MA, USA). JC-1 MitoMP detection kit was obtained from Dojindo (Kumamoto, Japan). Anti-α-Tubulin was purchased from Santa Cruz Biotechnology (Santa Cruz, CA, USA). Anti-p62 antibody was purchased from Sigma Chemical Co. (St. Louis, MO, USA). FITC Annexin V Apoptosis detection kit from BD pharmingen (San Diego, CA, USA). Cell Cycle and Apoptosis Analysis Kit was purchased from Yeasen Corporation (Shanghai, China). Secondary antibodies, anti-rabbit-horseradish peroxidase (HRP) and anti-mouse-HRP were from Jackson Immuno Research Laboratories (West Grove, PA, USA). Goat anti-Rabbit IgG (H+L) Highly Cross-Adsorbed Secondary Antibody, Alexa Fluor 647 and Alexa Fluor 488 were from ThermoFisher Scientific.

Toxoplasma gondii and Host Cells

RH and GFP-RH tachyzoites of *T. gondii* expressing green fluorescent protein were maintained by ARPE-19 cells at 5% CO_2 and 37°C. Infected cells were scraped, forcibly passed through a 27-gauge needle, and centrifuged at 1350 ×g for 10 min using Percoll (Sigma) to pellet the parasites.

The human RPE cell line ARPE-19 was purchased from the American Tissue Culture Collection (Manassas, VA, USA). The cells were routinely grown in Dulbecco's modified Eagle's medium/F12 (WelGENE, Daegu, South Korea) supplemented with 10% heat-inactivated fetal bovine serum (Gibco BRL, Grand Island, NY, USA), 2 mM glutamine, 100 U/mL penicillin, and 100 μg/mL streptomycin. Human foreskin fibroblast (HFF; ATCC, Manassas, VA) cells were cultured in DMEM supplemented with 10% FBS and 1% antibiotic-antimycotic solution (Gibco BRL). The cells were cultured at 37°C in 5% CO_2 and passaged every 3–4 days. ARPE-19 and HFF cells were used between passages 4 and 8 in this study.

Experimental Designs

ARPE-19 cells were seeded into 96-well plates [for the lactate dehydrogenase (LDH) assay], 12-well coverslips (for immunofluorescence), 6-well plates (for flow cytometry analysis), and 100-mm culture dishes (for Western blotting) at various densities and grown to confluence at 37°C in 5% CO_2.

To determine the optimal concentration of AgNPs for inducing apoptosis in human RPEs, ARPE-19 cells were treated with various concentrations of AgNPs for 24 h at 37°C in 5% CO_2. The cytotoxicity and apoptotic features of AgNP-treated ARPE-19 cells were evaluated by LDH assay, Western blotting, mitochondrial membrane potential (MMP) and immunofluorescence assay. To investigate the role of *T. gondii* in AgNP-induced cytotoxicity, ARPE-19 cells were treated with AgNPs alone or in combination with *T. gondii* at a multiplicity of infection (MOI) of 5 for 2 h. The cell cycle distribution, apoptotic features, ROS production, and activation of the AKT/mTOR and MAPK signaling pathways were evaluated by LDH assay, flow cytometry, Western blotting, immunofluorescence assay and specific commercial kits. To determine the mechanisms of anti-apoptosis induced by *T. gondii* in AgNP-treated ARPE-19 cells, NOX4 gene knockdown was performed by transfection with short interfering RNA (siRNA) duplexes specific for human NOX4, followed by treatment with 5 μg/mL AgNPs for 24 h. The apoptotic features and ROS production were again evaluated as described above.

To confirm the AgNP-induced cytotoxicity in ARPE-19 cells and its modulatory effects by *T. gondii* infection, the major experiments carried out in ARPE-19 cells were confirmed again using human foreskin fibroblast (HFF) cells and bone marrow-derived macrophages (BMDMs) isolated NOX4$^{-/-}$ mice. Untreated ARPE-19 and HFF cells and BMDMs were used as controls. Each experiment was performed at least three times in triplicate.

LDH Assay

An LDH assay was performed to quantify cytotoxicity. This assay was conducted using the CytoTox 96 Non-Radioactive Cytotoxicity Assay kit (Promega) according to the manufacturer's protocol. Briefly, 1×10^4 cells were seeded into 96-well plates and exposed to various concentrations of AgNPs (0, 0.2, 1, 5, 25, and 125 μg/mL) for 24 h in an incubator (5% CO_2, 90% relative humidity, 37°C). Next, 50 μL of the supernatant was transferred into a new 96-well plate and 50 μL of CytoTox 96 reagent was added and incubated for 30 min at room temperature. After incubation, the absorbance of the solution was measured immediately at 490 nm using a microplate reader (TECAN, Männedorf, Switzerland). LDH levels in the media were quantified and compared to control values according to the kit instructions.

Dead Cell Staining

The dead cells were visualized using the LIVE/DEAD Fixable Red Dead Cell Stain kit (Thermo Fisher Scientific) according to the manufacturer's instructions. Images were obtained using a confocal microscope (Leica TCS SP5 Microsystems, Wetzlar, Germany).

Western Blotting

After washing the cells with phosphate-buffered saline (PBS), proteins were extracted using the PRO-PREP Protein Extraction Solution (iNtRON Biotechnology, Seoul, Korea) and incubated with complete protease inhibitor cocktail (Roche, Basel, Switzerland) for 30 min on ice. After centrifugation at 14,000 ×g for 15 min at 4°C, the supernatant was collected and equal amounts of protein from each sample were separated by SDS-PAGE and transferred to a polyvinylidene difluoride membrane. The membranes were blocked in Tris-buffered saline (20 mM Tris, 137 mM NaCl, pH 7.6) containing 0.1% Tween-20 (TBST) and 5% skim milk. After washing once in TBST, the membranes were incubated overnight at 4°C with the primary antibodies diluted in TBST supplemented with 5% bovine serum albumin. Primary antibodies against the following factors were used: p-cdc2 (Tyr15), Cyclin A, Cyclin B1, Cyclin E2, p-Histone H3, Myt1, p21 Waf1/Cip1, p-Weel (Ser642), cleaved caspase-3, PARP, p62, LC3B, Bad, p-Bad, Bax, Bik, Bim, Bid, Bak, Puma, p-Bcl2 (Ser70), Bcl2, Bcl-xL, Mcl-1, cytochrome *c*, COX IV, p-AKT, AKT, p-mTOR, mTOR, p-p38, p38, p-ERK1/2, ERK1/2, p-JNK, JNK, NOX4, TP3, and α-tubulin. Following three consecutive washes in TBST, the membranes were incubated for 90 min with horseradish peroxidase-conjugated anti-mouse or anti-rabbit IgG (Santa Cruz Biotechnology) diluted 1:5000 with incubation buffer, as described above. The membrane was soaked with Immobilon Western Chemiluminescent HRP Substrate (Jackson ImmunoResearch Laboratories), and chemiluminescence was detected with a Fusion Solo System (Vilber Lourmat, Collegien, France). Band intensity was quantified using ImageJ software (NIH, Bethesda, MD, USA). The results were normalized to α-tubulin protein levels and are expressed as fold-changes compared to the control group.

Cell Cycle Transition and Apoptosis Determination

The cell cycle and apoptosis were evaluated using Cell Cycle and Apoptosis Analysis Kit (Yeasen Corporation) according to the manufacturer's instructions. Briefly, 1×10^6 cells were plated onto 60-mm cell culture dish cells and treated with different concentrations of AgNPs (0, 0.2, 1, 5, 25, and 125 μg/mL) for 24 h. The cells were fixed overnight in 70% ethanol at −20°C, incubated with RNase A solution at 37°C for 30 min, followed by staining with 400 mL propidium iodide (PI) solution at 4°C for 10 min in the dark. Stained cells were analyzed with a FACSCanto II flow cytometer (BD Biosciences, San Jose, CA, USA), and the sub-G1, G0/G1, S, and G2/M populations were analyzed with FlowJo software (Tree Star, Inc., Ashland, OR, USA).

Apoptosis Detection by FITC Annexin V/PI

An FITC Annexin V Apoptosis detection kit (BD Biosciences) was used to measure cell apoptosis. Briefly, the cells were plated into a six-well plate and treated with varying concentrations (0, 0.2, 1, 5, 25, and 125 μg/mL) of AgNPs for 24 h. Both floating and adherent cells were collected and washed twice with cold PBS. The cells were resuspended in 500 μL binding buffer and incubated with 5 μL Annexin V-FITC and 5 μL PI for 15 min at room temperature in the dark. Cell apoptosis was detected using a FACSCanto II flow cytometer.

Immunofluorescence Microscopy

Cells were seeded onto coverslips in 12-well plates at a density of 2×10^4 cells/well and incubated for 24 h. The cells were treated with AgNPs with or without *T. gondii* at the indicated time points. The cells were washed with PBS and fixed with freshly prepared 4% paraformaldehyde for 1 h at room temperature. After washing five times with PBS containing 0.3% Triton X-100 (PBS-T) for 10 min, the cells were incubated with primary antibodies (α-tubulin, cleaved

PARP, NOX4, cleaved caspase-3) for 2 h at room temperature. The cells were washed to remove excess primary antibody, and then incubated with the appropriate fluorescently labeled secondary antibodies (anti-rabbit Alexa Fluor 647 and anti-rabbit Alexa Fluor 488) for 2h at room temperature. After mounting with VECTASHIELD HardSet antifade mounting medium with DAPI (Vector Laboratories, Burlingame, CA, USA), fluorescence images were acquired using a confocal microscope (Leica).

Preparation of Mitochondrial and Cytosolic Fractions

Mitochondrial and cytosolic fractions of ARPE-19 cells were prepared as described previously.[22] For cytosolic extracts free of nuclei and mitochondria, the cells were washed in ice-cold PBS (pH 7.2) and then in hypotonic extraction buffer (HEB; 50 mM PIPES, 50 mM KCl, 5 mM EGTA, 2 mM $MgCl_2$, 1 mM dithiothreitol, 0.1 mM phenylmethylsulfonyl fluoride, pH 7.4) and harvested by centrifugation. Pellets were resuspended in HEB and lysed with a Dounce homogenizer. These cell lysates were then centrifuged at 100,000 ×*g* for 60 min at 4°C, and the supernatants were flash-frozen in cold ethanol, aliquoted, and stored at −80°C.

Mitochondrial fractions were prepared by washing the cells in ice-cold PBS and then resuspending them in an isotonic homogenization buffer (10 mM Tris-HCl, pH 7.5, 0.25 M sucrose, 10 mM KCl, 1 mM EDTA, 1 mM dithiothreitol, 0.1 mM phenylmethylsulfonyl fluoride, EDTA-free complete cocktail of protease inhibitors [Roche]). After 60 strokes in a Dounce homogenizer, unbroken cells were removed by centrifugation at 1000 ×*g* for 10 min, and the supernatants were centrifuged at 14,000 ×*g* for 20 min. The supernatants were collected as the mitochondrial fraction. The expression of cytochrome *c* expression was determined by Western blotting. COX IV and α-tubulin were used as mitochondria and cytosol markers, respectively.

Confocal Microscopy of JC-1

The JC-1 MitoMP detection kit (Dojindo, Kumamoto, Japan) was used to measure mitochondrial stability in ARPE-19 cells. ARPE-19 cells were seeded onto coverslips in 12-well plates at a density of 2×10^4 cells/well and incubated for 24 h. The cells were treated with AgNPs with or without *T. gondii* at the indicated time points. The cells were then incubated with 4 μM JC-1 fluorescence dye at 37°C for 30 min and rinsed three times with HBSS. The samples were observed using a confocal laser scanning microscope.

Measurement of ROS Generation

MitoSOX and CellROX were used to measure either mitochondrial matrix superoxide or intracellular ROS levels, respectively. Briefly, the cells were incubated with 5 μM MitoSOX reagent for 10 min or 5 μM CellROX reagent for 30 min at 37°C and then analyzed by flow cytometry or with a confocal microscope.

siRNA Transfection

Cells were transfected with siRNA duplexes specific for human NOX4 using Lipofectamine RNAiMAX (Life Technologies, Carlsbad, CA, USA) according to the manufacturer's protocol. Briefly, the cells were seeded into 6-well plates, grown for 24 h (70% confluence), and then transfected with 20 nM NOX4-specific siRNA or negative control siRNA (Santa Cruz Biotechnology) for 48 h. Next, the cells were pre-infected with GFP-RH *T. gondii* at a MOI of 5 for 2 h and treated with or without 5 μg/mL AgNPs for 24 h. Knockdown efficiency was determined by qRT-PCR and Western blotting.

Quantitative Real-Time Polymerase Chain Reaction (qRT-PCR)

Total RNA was extracted using TRIzol Reagent (Invitrogen, Carlsbad, CA, USA) and RNA was transcribed into cDNA using M-MLV reverse transcriptase (Invitrogen) as described by the manufacturer. qRT-PCR was performed using Power SYBR® Green PCR Master Mix (Applied Biosystems, Foster City, CA, USA). The sequences of the primers used were as follows: NOX4 (forward: 5′-GCC AGA GTA TCA CTA CCT CCA C-3′; reverse: 5′-CTC GGA GGT AAG CCA AGA GTG T-3′) and HPRT1 (forward: 5′-GAC CAG TCA ACA GGG GAC AT-3′; reverse: 5′-CTG CAT TGT TTT GCC AGT GT-3′). All reactions were performed with an ABI 7500 Fast Real-Time PCR system (Applied Biosystems) under the following conditions: 95°C for 10 min, followed by 40 cycles of 95°C for 15 s and 60°C for 60 s. Relative NOX4 gene expression levels were quantified based on the cycle threshold (Ct) values and normalized to the reference gene hypoxanthine phosphoribosyltransferase 1 (HPRT1). Each sample was measured in triplicate, and gene expression levels were calculated using the $2^{-\Delta\Delta Ct}$ method.

Generation of Bone-Marrow-Derived Macrophages (BMDMs)

Bone marrow-derived macrophages were isolated from wild-type and NOX4 knockout mouse and differentiated for 5–7 days in medium containing macrophage colony-stimulating factor, as described previously.[25] The culture

medium consisted of Dulbecco's modified Eagle's medium (Life Technologies) supplemented with 10% heat-inactivated fetal bovine serum, 1 mM sodium pyruvate, 50 U/mL penicillin, 50 μg/mL streptomycin, and 5×10^{-5} M β-mercaptoethanol.

Statistical Analysis

All assays were performed using at least three times and in triplicate. Data were expressed as the means ± standard deviation (SD). Statistical analysis of the data was performed using unpaired, two-tailed Student's *t*-tests with Bonferroni adjustment or ANOVA for multiple comparisons. A *P*-value of less than 0.05 was considered to indicate statistical significance.

Results

AgNP Treatment Induced Morphological Changes in ARPE-19 Cells

To investigate the effects of AgNPs on ARPE-19 cell morphology, the cells were treated with various concentrations of AgNPs for 24 h. The integrity of the microtubule network was assessed by immunofluorescence microscopy using an α-Tubulin antibody to stain cellular microtubules with DAPI for DNA. Analysis of immunofluorescence staining of ARPE-19 cells was displayed a well-developed array of hair-like microtubule networks of slim fibrous microtubules (green) wrapped around the cell nucleus (blue) in control cells. In contrast, cells treated with AgNPs showed a tubulin staining pattern that was diffuse and disorganized. AgNP-treated cells showed morphological changes with condensed chromatin, nucleus fragmentation, and cellular shrinkage, whereas untreated cells grew well with a clear complete cytoskeleton (Figure 1A). Additionally, fluorescence images were acquired after staining of dead cells using the Red Dead Cell Stain kit. ARPE-19 cell death was clearly induced by treatment with 1 μg/mL AgNPs and dead cell numbers were significantly increased by AgNPs in a concentration-dependent manner (Figure 1B). These data indicate that AgNPs treatment altered the ARPE-19 cell morphology and induced cell death.

AgNPs Dose-Dependently Induced Cytotoxicity and Sub-G1 Phase Cell Accumulation in ARPE-19 Cells

To evaluate the effects of AgNPs on ARPE-19 cell cytotoxicity, the cells were treated with various concentrations of AgNPs for 24 h and then subjected to a LDH assay. In the presence of 0, 0.2, 1, 5, 25, and 125 μg/mL AgNPs, cytotoxicity of ARPE-19 cells is shown at 3.96 ± 0.58%, 8.26 ± 1.02%, 16.69 ± 1.78%, 26.5 ± 1.16%, 34.6 ± 2.79%, and 43.66 ± 1.67%, respectively (Figure 2A). These data indicate that AgNPs treatment induced cytotoxicity in ARPE-19 cells.

Next, we evaluated the effects of AgNPs on cell cycle phase distribution in ARPE-19 cells by flow cytometry. The analysis of the cell cycle profile of ARPE-19 cells showed that the fractions of cells in sub-G1 and S phase were significantly increased in AgNP-treated cells as compared to control, whereas the fraction of G0/G1 phase cells was decreased. Especially, treatment with AgNPs clearly increased the sub-G1 fraction in a dose-dependent manner in ARPE-19 cells. The relative percentages of sub-G1 phase cells were progressively increased from 3.77% in untreated cells to 8.53% and 17.95% in AgNP-treated ARPE-19 cells at 5 or 25 μg/mL AgNPs, respectively (Figure 2B). We also assessed various proteins related to cell cycle by Western blotting analysis. As shown in (Figure 2C), the levels of phospho-cdc2 (Tyr15), cyclin A2, phospho-histone H3 (Ser10), and p21 Waf1/Clip were elevated in ARPE-19 cells in response to 5 μg/mL AgNPs, whereas the levels of cyclin E2 were decreased. The Myt1 and phospho-Wee1 (Ser642) protein levels showed no difference. Taken together, AgNPs induced cell cycle dysregulation in ARPE-19 cells, and the increase of subG1 cell population indicated the increase of apoptotic cell death by AgNPs treatment.

AgNPs Dose-Dependently Induced Apoptosis and Autophagy in ARPE-19 Cells

To evaluate whether the cytotoxicity by AgNPs on ARPE-19 cells resulted from apoptotic cell death, cleavages of caspase-3 and PARP were analyzed by Western blotting. The cleavages of caspase-3 and PARP became apparent starting at 0.2 μg/mL AgNPs. AgNPs induced cleavages of caspase-3 and PARP, dose-dependently (Figure 3A). Furthermore, flow cytometric analysis confirmed that both early and late apoptoses were significantly increased. The percentages of early apoptotic cells, which were appeared in the annexin V^+/PI^- fraction, were significantly increased from 1 μg/mL AgNPs as compared with control (Figure 3B).

To determine whether AgNPs treatment resulted in autophagy, the levels of autophagy-related proteins were investigated. Western blotting results showed that as the concentration of AgNPs increased, the protein levels of LC3B significantly increased, suggesting that autophagosome formation was induced. Interestingly, the protein levels of p62, a selective receptor of autophagy substrates, were dose-dependently decreased with AgNP treatment

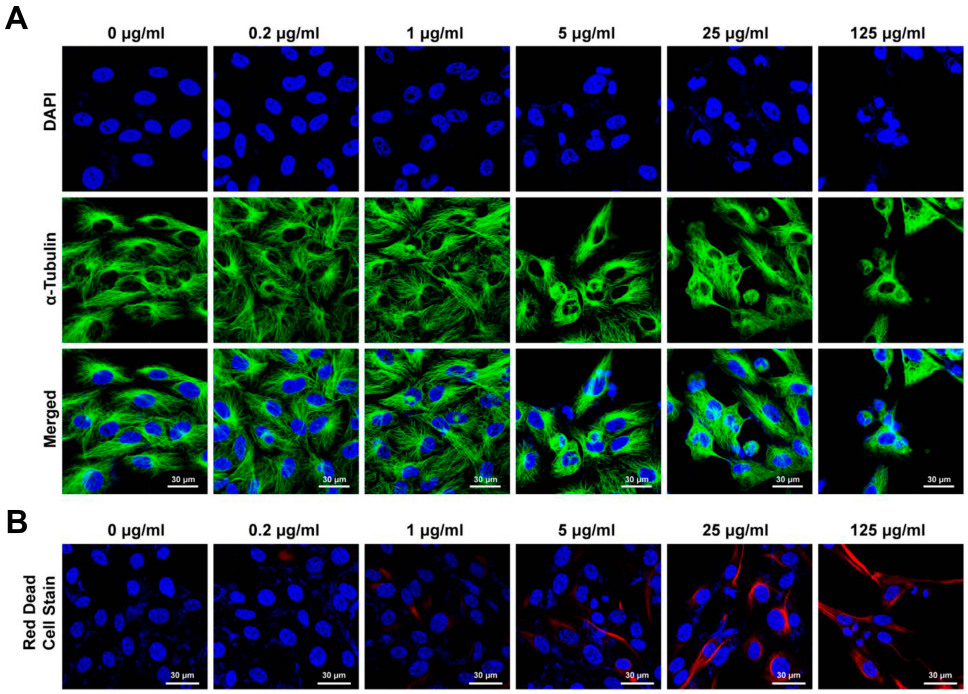

Figure 1 AgNPs treatment changed the morphology of ARPE-19 cells. ARPE-19 cells were grown for 24 h and treated with various concentrations of AgNPs for 24 h. (**A**) ARPE-19 cells were fixed and probed against α-tubulin (green). The cells were counterstained with DAPI (blue) and visualized by confocal microscopy. (**B**) Fluorescence images were acquired after staining of dead cells using the Red Dead Cell Stain kit. Similar results were obtained in three independent experiments.
Abbreviations: AgNPs, silver nanoparticles; DAPI, 4′,6-diamidino-2-phenylindole

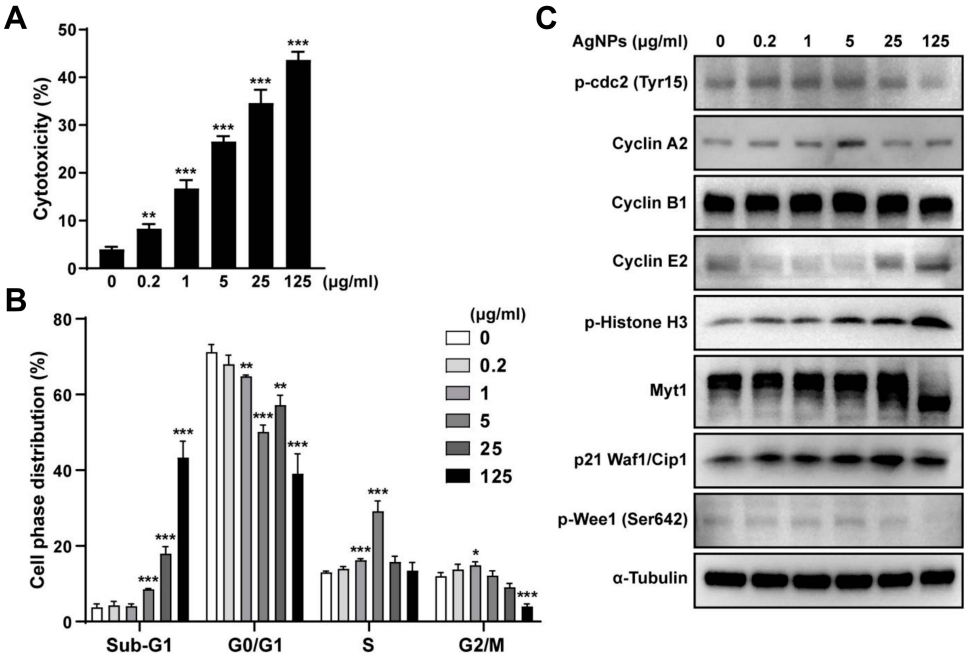

Figure 2 AgNPs induced cytotoxicity and cell cycle arrest of ARPE-19 cells. (**A**) LDH level in the media was measured after treatment with AgNPs for 24 h. The percentage of cytotoxicity was represented as the mean ± standard deviations of at least 3 independent experiments. (**B**) Following treatment with AgNPs at the indicated concentrations for 24 h, the ratio (%) of the cell distribution in the indicated stages was analyzed by flow cytometry and compared to that in non-treated cells. (**C**) Expression of proteins related to the cell cycle was detected by Western blot analysis, with α-tubulin used as the loading control. Images show chemiluminescent detection of the blots, which are representative of three independent experiments. *$P < 0.05$; **$P < 0.01$; ***$P < 0.001$, as compared to the control group.
Abbreviations: AgNPs, silver nanoparticles; MOI, multiplicity of infection; LDH, lactate dehydrogenase; cdc2, cell division control protein; Myt1, myelin transcription factor 1

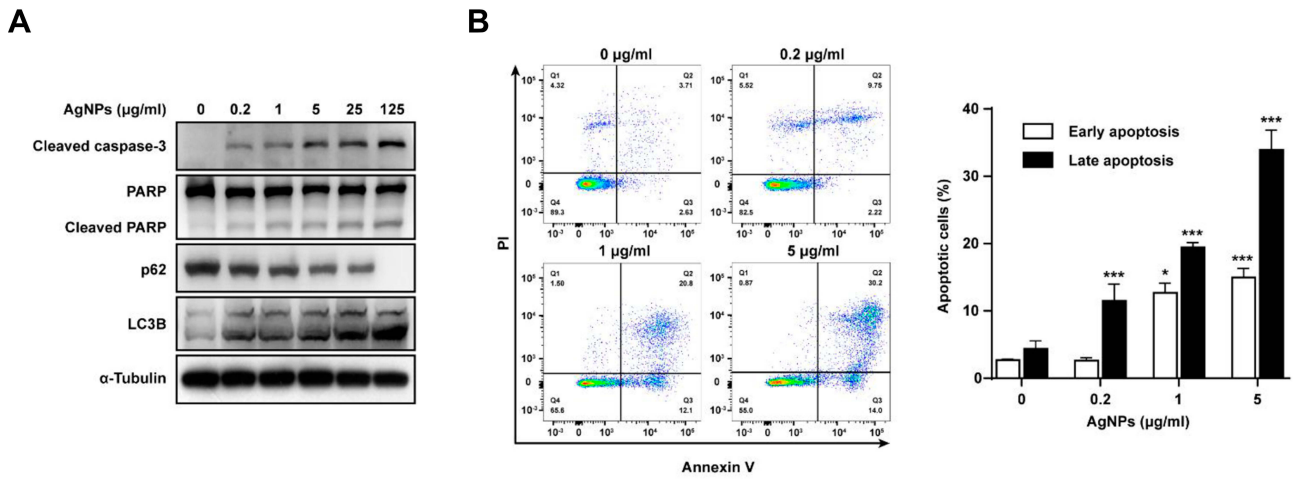

Figure 3 AgNPs induced apoptosis and autophagy of ARPE-19 cells. ARPE-19 cells were treated with various concentrations of AgNPs for 24 h. (**A**) Protein levels of cleaved caspase-3 and PARP, p62, and LC3B were determined by Western blotting. (**B**) Ratio of apoptosis was measured and analyzed by Annexin V-FITC/PI staining and flow cytometry. Data are presented as the means ± standard deviation (SD). Similar results were obtained in three independent experiments. *, $P < 0.05$; ***, $P < 0.001$, as compared to the control group.

Abbreviations: AgNPs, silver nanoparticles; MOI, multiplicity of infection; PARP, poly (ADP-ribose) polymerase; LC3, microtubule-associated protein 1A/1B-light chain 3; FITC, fluorescein isothiocyanate; PI, propidium iodide

(Figure 3A). As shown in (Figure 3B), ARPE-19 cells treated with 0.2, 1 and 5 μg/mL AgNPs showed increased late apoptotic rates to 11.52 ± 2.48%, 19.43 ± 0.71%, and 33.9 ± 2.95%, respectively, whereas this rate in the control group was 4.37 ± 1.19%. These results suggest that AgNPs induced caspase-dependent apoptosis and autophagic cell death in ARPE-19 cells. Thus, treatment with 5 μg/mL AgNPs for 24 h was used to induce AgNP-mediated ARPE-19 cell apoptosis in subsequent experiments.

T. gondii Pre-Infection Inhibited AgNP-Induced Apoptosis in ARPE-19 Cells

To assess whether *T. gondii* infection exerts modulatory effects on AgNP-induced apoptosis of ARPE-19 cells, ARPE-19 cells were first infected with *T. gondii* at MOI of 5 for 2 h, and uninfected parasites were washed out. Next, the infected ARPE-19 cells were treated with 5 μg/mL AgNPs for 24 h. Surprisingly, *T. gondii*-infected ARPE-19 cells inhibited AgNP-induced apoptosis. Western blot analysis showed that cleaved caspase-3 (17 kDa) was detected in AgNP-treated cells. PARP was also cleaved into an 89-kDa fragment in AgNP-treated cells. However, the levels of these fragments were prominently decreased by *T. gondii* pre-infection in AgNP-treated cells (Figure 4A). In addition, flow cytometric analysis confirmed that *T. gondii* pre-infection significantly inhibited AgNP-induced late apoptotic rates (Figure 4B). To confirm the changes in nuclei and PARP cleavage induced by AgNPs, we performed cleaved PARP staining to detect nuclear DNA damage. As shown in (Figure 4C), the nuclei in cells infected with *T. gondii* were intact, round, and uniformly stained. However, AgNPs treatment led to manifest nuclear shrinkage/condensation and nuclear fragmentation in cells uninfected with *T. gondii*. Cleaved PARP-positive cells were observed following AgNPs treatment. However, cleaved PARP-positive cells were significantly decreased in cells pre-infected with *T. gondii* after treatment with AgNPs (Figure 4C). Taken together, these data show that *T. gondii* pre-infection suppressed the caspase-3 activation, PARP degradation and apoptotic rates in AgNP-treated ARPE-19 cells.

T. gondii Pre-Infection Inhibited AgNP-Induced Mitochondrial Apoptosis in ARPE-19 Cells

To determine the mechanism underlying *T. gondii*-dependent suppression of AgNP-induced apoptosis, we assessed the expression of pro-apoptosis and pro-survival Bcl-2 family proteins. AgNPs treatment significantly and dose-dependently increased Bax, Bik, and Bim pro-apoptosis Bcl-2 protein levels (Figure 5A). However, AgNPs treatment did not significantly affect phospho-Bcl2 (Ser70), Bcl-2, Bcl-xL, and Mcl-1 pro-survival Bcl-2 family protein levels (Figure 5B).

Bcl-2 plays an important role in the maintenance of mitochondria integrity by preventing apoptosis-induced cytochrome *c* release, and cytochrome *c* is involved in activating downstream

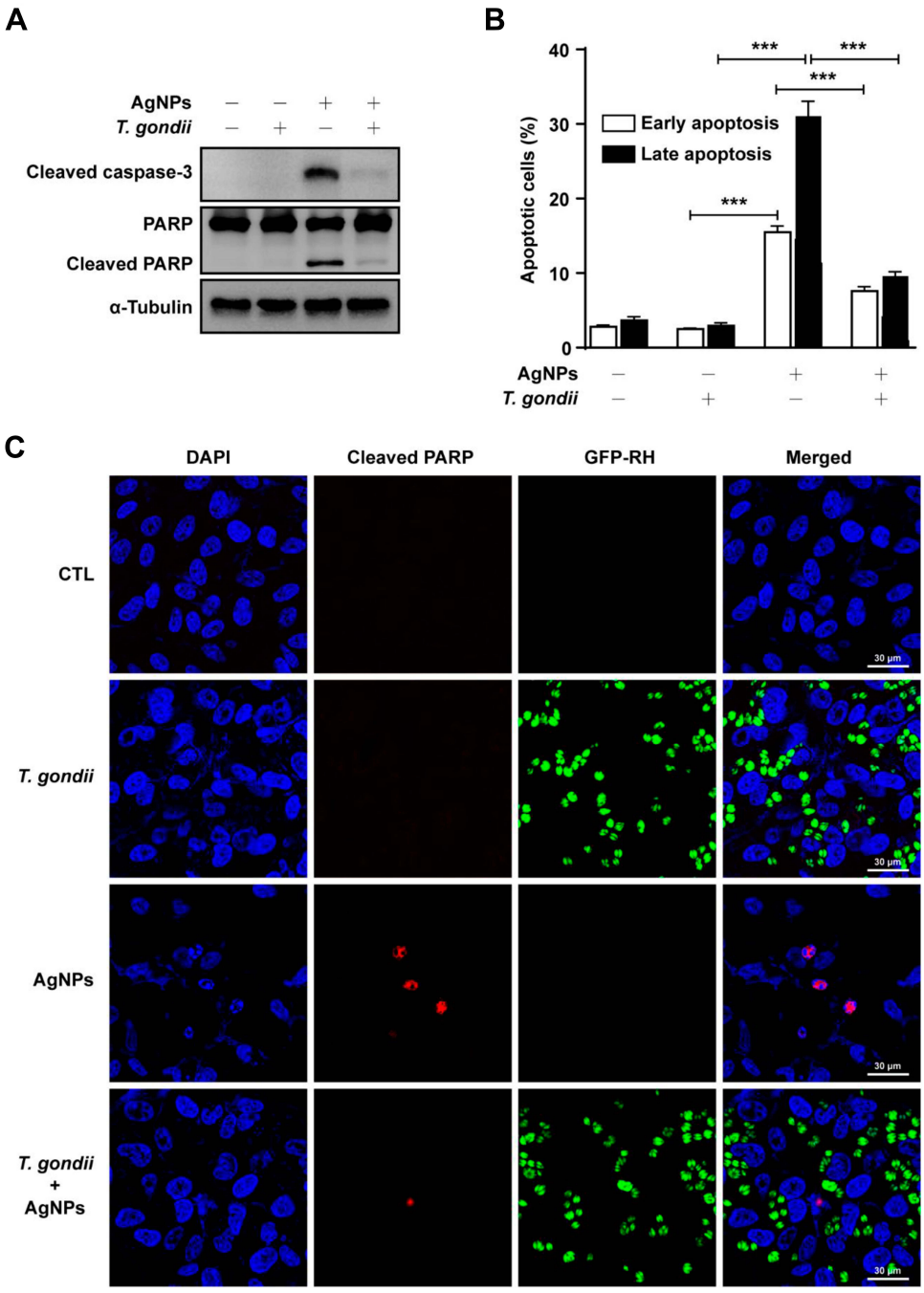

Figure 4 *T. gondii* inhibited AgNP-induced apoptosis of ARPE-19 cells. ARPE-19 cells were pre-infected with *T. gondii* at MOI 5 for 2 h, and then treated with 5 μg/mL AgNPs for 24 h. (**A**) The protein levels of cleaved caspase-3 and PARP were determined by Western blotting. (**B**) Ratio of apoptosis was measured and analyzed by Annexin V-FITC/PI staining and flow cytometry. Data are presented as the means ± standard deviation (SD). Similar results were obtained in three independent experiments. ***, $P < 0.001$, as compared to the uninfected AgNP-treated group or normal control group. (**C**) Apoptosis was detected by cleaved PARP staining.

Abbreviations: AgNPs, silver nanoparticles; MOI, multiplicity of infection; PARP, poly (ADP-ribose) polymerase; MOI, multiplicity of infection; FITC, fluorescein isothiocyanate; PI, propidium iodide; DAPI, 4′,6-diamidino-2-phenylindole

caspases that trigger apoptosis.[18,22,23] Therefore, cytochrome *c* levels were analyzed in the mitochondrial and cytosolic fractions. AgNPs induced the release of cytochrome *c* from the mitochondria into the cytoplasm. In contrast, cytochrome *c* release was prevented by *T. gondii* pre-infection in AgNP-treated cells (Figure 5C). Similarly, AgNPs induced upregulation of Bax, Bik, and Bim pro-apoptosis Bcl-2 family protein levels, which was attenuated by *T. gondii* pre-infection (Figure 5D). Next, to evaluate whether *T. gondii* pre-infection inhibited AgNP-induced apoptotic features related to mitochondrial membrane integrity, we utilized JC-1, an indicator of MMP. As JC-1 dye exhibits potential-dependent accumulation in the mitochondria with a fluorescence shift from green

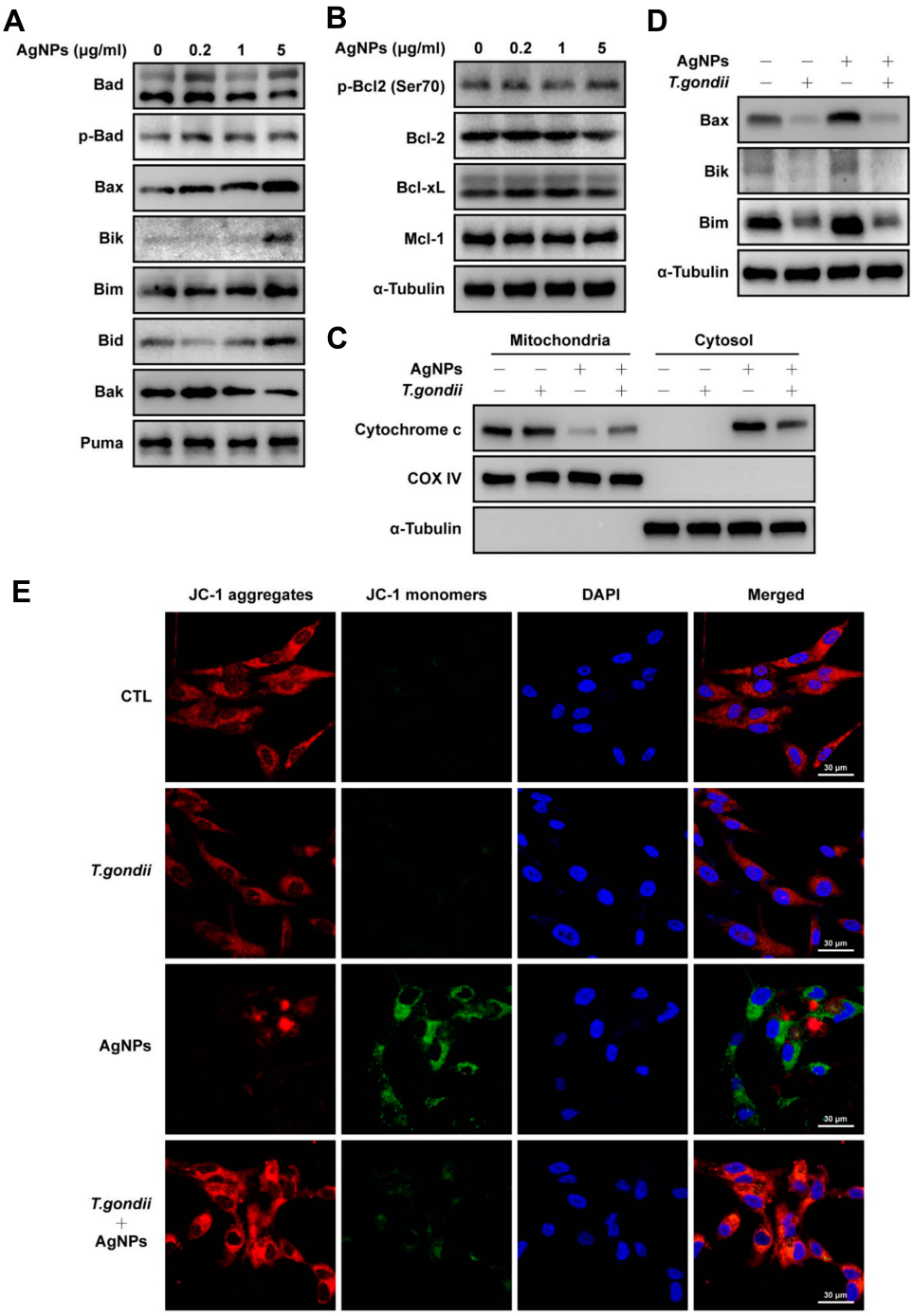

Figure 5 *T. gondii* inhibited AgNP-induced mitochondrial apoptosis in ARPE-19 cells. ARPE-19 cells were pre-infected with *T. gondii* at MOI 5 for 2 h, and then treated with or without 5 μg/mL AgNPs for 24 h. (**A,B,D**) Pro-apoptosis (**A,D**) and pro-survival (**B**) Bcl-2 family protein levels were evaluated by Western blotting. (**C**) Mitochondrial and cytosolic fractions were analyzed for the expression of cytochrome *c*. COX IV and α-Tubulin were used as markers of mitochondria and cytosol, respectively. (**E**) JC-1 staining was observed by confocal imaging. In JC-1 stained cells, red fluorescence is visible in cells with high mitochondrial membrane potential, while green fluorescence of JC-1 monomer is present in cells with low mitochondrial potential. All data shown are representative of 3 independent experiments with similar results.

Abbreviations: AgNPs, silver nanoparticles; MOI, multiplicity of infection; Bcl-2, B-cell lymphoma 2; Bad, Bcl-2-associated death promoter; Bax, Bcl-2-associated X protein; Bik, BCL2-interacting killer; Bim, Bcl-2-like protein 11; Bid, BH3 interacting domain death agonist; Bak, BCL2-antagonist/killer; Puma, p53 upregulated modulator of apoptosis; Bcl-xL, B-cell lymphoma-extra large; Mcl-1, myeloid cell leukemia 1; COX, Cytochrome c oxidase; JC-1, 5.5′,6,6′-Tetrachloro-1,1′,3,3′-tetraethylimidacarbocyanine iodide; DAPI, 4′,6-diamidino-2-phenylindole

(488 nm) to red (561 nm), mitochondrial depolarization is indicated by a decrease in the red:green fluorescence intensity ratio. AgNPs treatment displayed a greatly decreased MMP as evidenced by the reduction in red and increase in green JC-1 fluorescence compared to control cells. However, this effect was suppressed by *T. gondii*-pre-infection (Figure 5E). These results indicate that AgNPs

impaired the MMP and induced mitochondrial apoptosis in ARPE-19 cells, whereas *T. gondii* pre-infection inhibited AgNP-induced apoptotic features in the mitochondria of ARPE-19 cells.

AgNP-Induced Sub-G1 Phase Cell Accumulation and JNK Signaling Activation in ARPE-19 Cells Were Suppressed by *T. gondii* Pre-Infection

To investigate the signaling pathways involved in AgNP-induced apoptosis of ARPE-19 cells, we analyzed the phosphorylation of AKT, mTOR, p38 MAPK, ERK1/2, and JNK in AgNP-treated ARPE-19 cells using phospho-specific antibodies. AgNPs induced a strong increase in p-JNK levels; however, p-AKT, p-mTOR, p-p38 MAPK, and p-ERK1/2 levels were dose-dependently decreased in ARPE-19 cells after treatment with AgNPs compared to in control cells (Figure 6A). We also assessed the effects of *T. gondii* pre-infection on the AKT/mTOR and MAPK signaling pathways in ARPE-19 cells treated with AgNPs. AgNP-induced activation of p-JNK was completely suppressed by *T. gondii* pre-infection, whereas AgNP-reduced p-AKT, p-mTOR, p-p38 MAPK and p-ERK1/2 levels were slightly elevated by *T. gondii* pre-infection. There were no significant changes in the total protein levels of AKT, mTOR, p38, ERK1/2, JNK, and p38 MAPK in the cells during these treatments (Figure 6B).

We further evaluated the role of the JNK pathway in the AgNP-induced sub-G1 cell cycle distribution. The relative percentages of sub-G1 phase cells were significantly decreased from 13.29% in AgNP-treated cells to 5.13% in *T. gondii* pre-infected AgNPs-treated ARPE-19 cells. Similarly, JNK inhibitor, SP600125-pretreatment significantly reduced sub-G1 cell population to 5.73% compared with AgNP-treated ARPE19 cells (Figure 6C). Also, *T. gondii* pre-infection significantly reduced AgNP-induced cyclin A2, phospho-histone H3, and p21 Waf1/Clip protein levels (Figure 6D). These results indicate that AgNP-induced sub-G1 phase cell accumulation of ARPE-19 cells was strongly associated with activation of the JNK signaling pathway, and cell cycle dysregulation including sub-G1 phase cell accumulation was suppressed by *T. gondii* pre-infection.

T. gondii Pre-Infection Inhibited AgNP-Induced Mitochondrial ROS Generation in ARPE-19 Cells

According to previous studies, mitochondrial ROS may be involved in the activation of caspases and MAPKs[18,22,23] and is responsible for the apoptosis-inducing effects of AgNPs.[3–7] We evaluated whether *T. gondii* pretreatment suppressed AgNP-triggered intracellular ROS production in ARPE-19 cells. The cells were pre-infected with *T. gondii* at MOI 5 for 2 h and treated with or without 5 μg/mL AgNPs for 24 h. We then evaluated ROS production using MitoSOX red mitochondrial superoxide indicator that specifically detects ROS produced within mitochondria. Histograms of the results of FACS analysis showed that treatment with 5 μg/mL AgNPs for 24 h significantly increased the percentage of ROS-positive cells, which was reversed by pretreatment with *T. gondii* pre-infection (Figure 7A and B). Similarly, confocal microscopic imaging showed that the MitoSOX red fluorescence signal in the cells treated with AgNPs showed increased mitochondrial ROS production compared to control cells, which was significantly inhibited by pretreatment with *T. gondii* (Figure 7C and D). These results indicate that AgNPs induced ROS-mediated mitochondrial apoptosis in ARPE-19 cells, which can be suppressed by *T. gondii* pre-infection.

T. gondii Pre-Infection Inhibited AgNP-Induced NOX4 Production in ARPE-19 Cells

NOX4 is a major NOX isoform and strongly induces ROS generation in ARPE-19 cells.[26] To investigate whether *T. gondii* regulates host NOX4 expression to inhibit AgNP-induced ROS generation, ARPE-19 cells were pre-infected with GFP-RH *T. gondii* at MOI 5 for 2 h and then treated with or without 5 μg/mL AgNPs for 24 h. We found that AgNPs significantly increased NOX4 protein levels, whereas *T. gondii* pre-infection significantly attenuated AgNP-induced NOX4 expression; however, AgNPs did not affect TP3 protein levels (Figure 8A). Similar results were also detected for *T. gondii*-regulated NOX4 mRNA levels by qRT-PCR analysis (Figure 8B). These results were confirmed by anti-NOX4 antibody staining. The NOX4 red fluorescence signal in the cells treated with AgNPs showed increased NOX4 protein expression compared to control cells, which was significantly inhibited by pretreatment with *T. gondii* (Figure 8C). These results suggest that NOX4 was involved in the AgNP-induced ROS generation, and *T. gondii* pre-infection attenuated AgNP-induced NOX4 expression.

NOX4 Was Responsible for AgNP-Induced Mitochondrial Apoptosis and ROS Generation in ARPE-19 Cells

To evaluate the role of NOX4 in AgNP-induced ROS generation, ARPE-19 cells which had been incubated for 48 h after transfection with control siRNA or specific

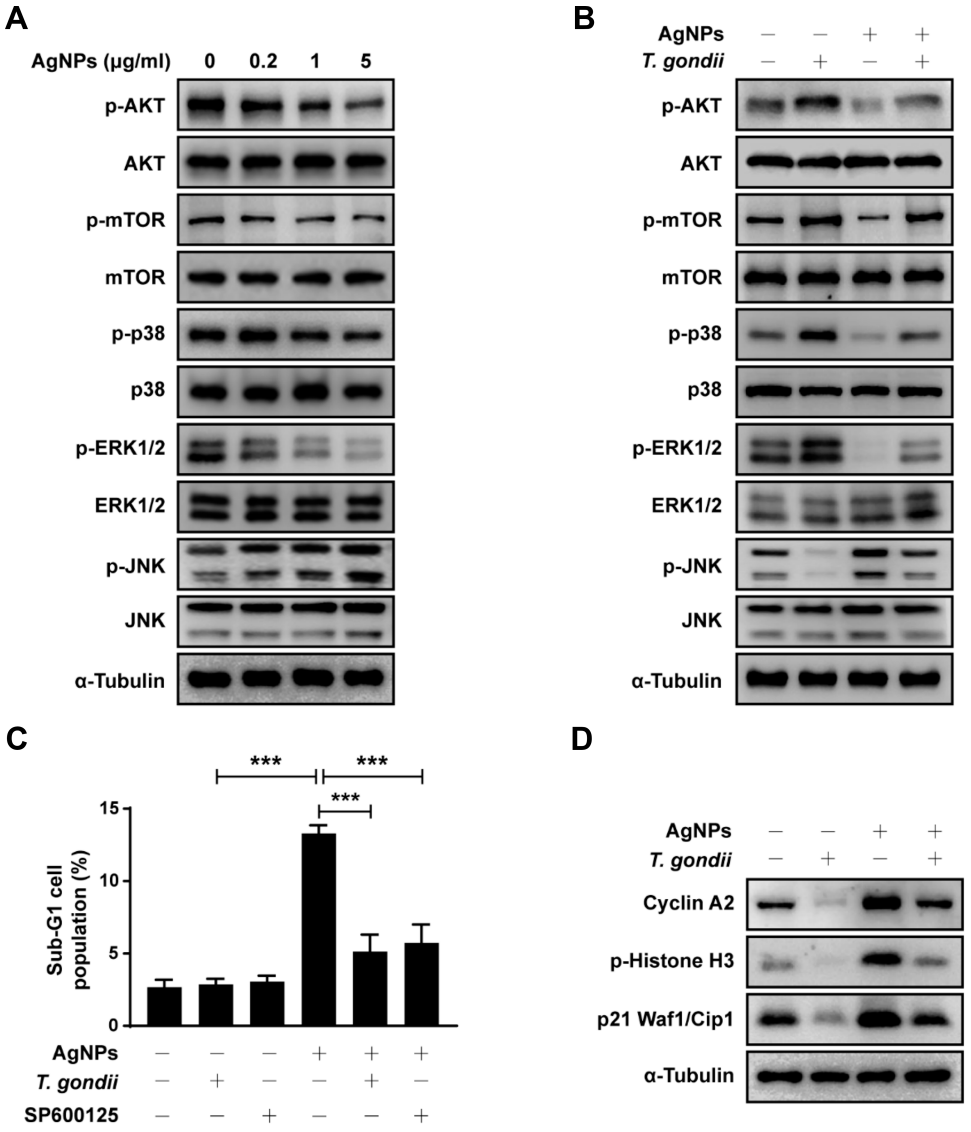

Figure 6 *T. gondii* inhibited AgNP-induced sub-G1 phase cell accumulation and JNK phosphorylation in ARPE-19 cells. (**A**) ARPE-19 cells were treated with various concentrations of AgNPs for 24 h. The phosphorylation levels of AKT, mTOR, and MAPKs were assessed by Western blot analysis. (**B**) ARPE-19 cells were pre-infected with *T. gondii* at MOI 5 for 2 h and then treated with 5 μg/mL AgNPs at the indicated time points. Phosphorylation levels of AKT, mTOR, and MAPKs were assessed by Western blot analysis. Anti-α-Tubulin was used as an internal control. (**C**) ARPE-19 cells were preincubated with the 30 μM SP600125 for 1 h and infected with or without *T. gondii* at MOI 5 for 2 h, and then treated with 5 μg/mL AgNPs for 24 h. Sub-G1 cell population was analyzed by flow cytometry. ***, $P < 0.001$, as compared to the indicated control group. (**D**) Proteins related to cell cycle were detected by Western blot analysis, and α-Tubulin was used as a loading control. Similar results were obtained in three independent experiments.

Abbreviations: AgNPs, silver nanoparticles; MOI, multiplicity of infection; AKT, protein kinase B; mTOR, mammalian target of rapamycin; MAPK, mitogen-activated protein kinase; p38, p38 mitogen-activated protein kinases; ERK, extracellular signal-regulated kinase; JNK, c-Jun N-terminal kinases; p21, cyclin-dependent kinase inhibitor 1

NOX4 siRNAs were treated with 5 μg/mL AgNPs for 24 h and then total ROS levels were detected by measuring the CellROX deep red fluorescence signals. Confocal microscopy imaging revealed an increase in the CellROX red fluorescence signal in control siRNA-transfected cells treated with AgNPs; however, AgNP-induced total ROS level was suppressed in NOX4 knockdown cells (Figure 9A).

Next, the role of NOX4 in AgNP-induced apoptosis was evaluated. According to Western blot analysis, the expression levels of NOX4 and cleaved PARP were increased in cells treated with AgNPs (Figure 9B). Similarly, confocal microscopy revealed that the expression of active caspase-3 (cleaved caspase-3) was increased in control siRNA-transfected cells treated with AgNPs compared to in siRNA-transfected cells. NOX4 knockdown cells prevented the AgNP-induced expression of cleaved caspase-3 (Figure 9D). Interestingly, similar results were observed for mitochondrial ROS levels according to MitoSOX red staining. Histograms of the

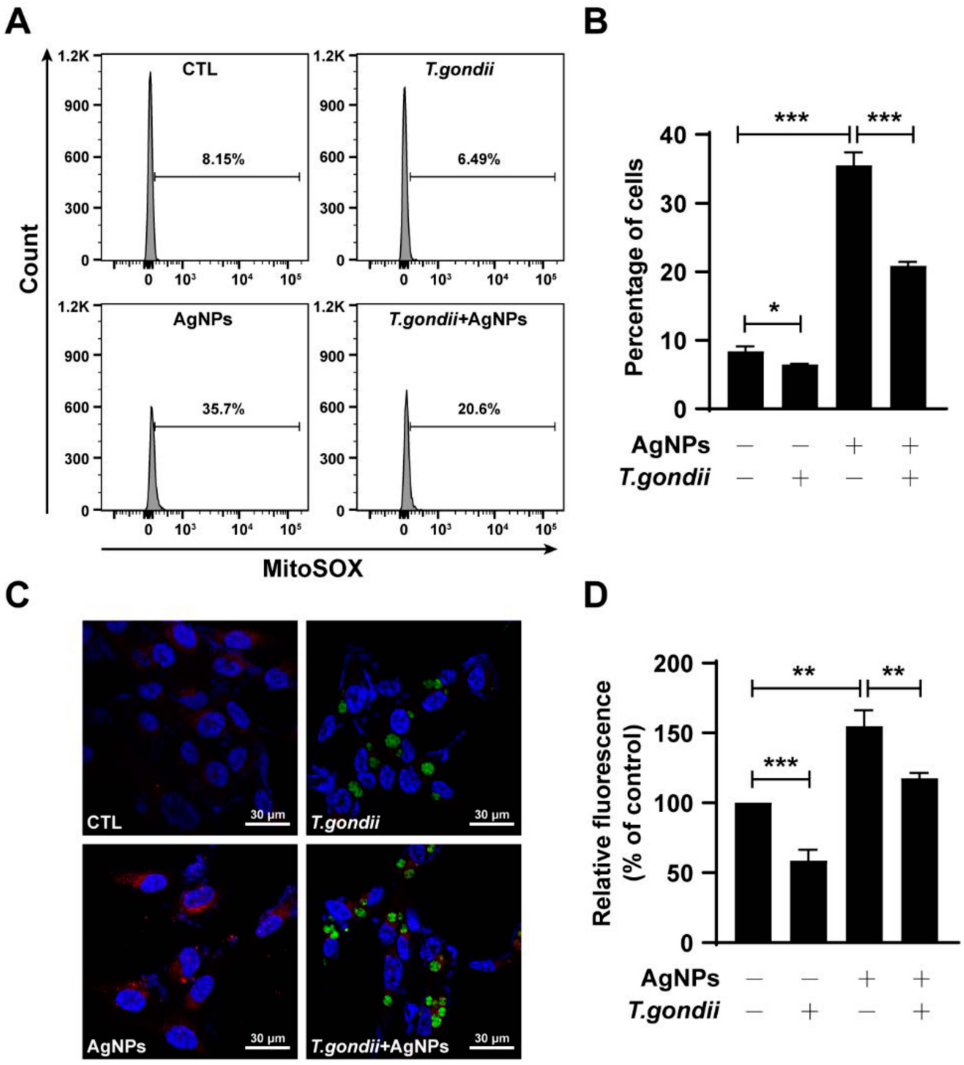

Figure 7 *T. gondii* inhibited AgNP-induced mitochondrial ROS production in ARPE-19 cells. The cells were loaded with MitoSOX red (5 μM for 30 min) and mitochondrial ROS were detected by flow cytometry and under a confocal microscope. (**A**) Representative histograms of flow cytometry showing the fluorescent intensity of MitoSOX red. (**B**) Relative fluorescence intensity of the population of MitoSOX-stained cells corresponding to A. (**C**) Representative confocal images of ROS generation in the cells, as MitoSOX red fluorescence. (**D**) Quantitative analysis of MitoSOX red fluorescence. Data are expressed as the mean ± standard deviation of three experiments. *$P < 0.05$, **$P < 0.01$, ***, $P < 0.001$, as compared to the control group.

Abbreviations: AgNPs, silver nanoparticles; ROS, reactive oxygen species

results of FACS analysis showed that the percentage of ROS-positive cells was significantly increased for control siRNA-transfected cells in the presence of 5 μg/mL AgNPs for 24 h, which was significantly inhibited by NOX4 knockdown (Figure 9C).

Finally, NOX4 in AgNP-induced mitochondrial apoptosis was confirmed by JC-1 staining. In control siRNA-transfected cells, AgNPs treatment greatly decreased MMP as evidenced by reduced red and increased green JC-1 fluorescence. However, this phenomenon was reversed by NOX4 siRNA transfection (Figure 9E). These results suggest that NOX4 was involved in AgNP-induced mitochondria apoptosis and ROS generation in ARPE-19 cells.

T. gondii Pre-Infection Prevented AgNP-Induced Apoptosis by Suppressing NOX4-Dependent ROS Generation in Murine ex vivo Model

To further confirm the anti-apoptosis effect by *T. gondii* infection through suppression of NOX4-dependent ROS generation, BMDMs were isolated from wild-type and NOX4 knockout mice. BMDM cells were pre-infected with *T. gondii* at MOI 5 for 2 h, and the uninfected parasites were washed out, followed by treatment with 5 μg/mL AgNPs for 24 h. In wild mice BMDMs, cleaved caspase-3 positive cells were observed following AgNPs

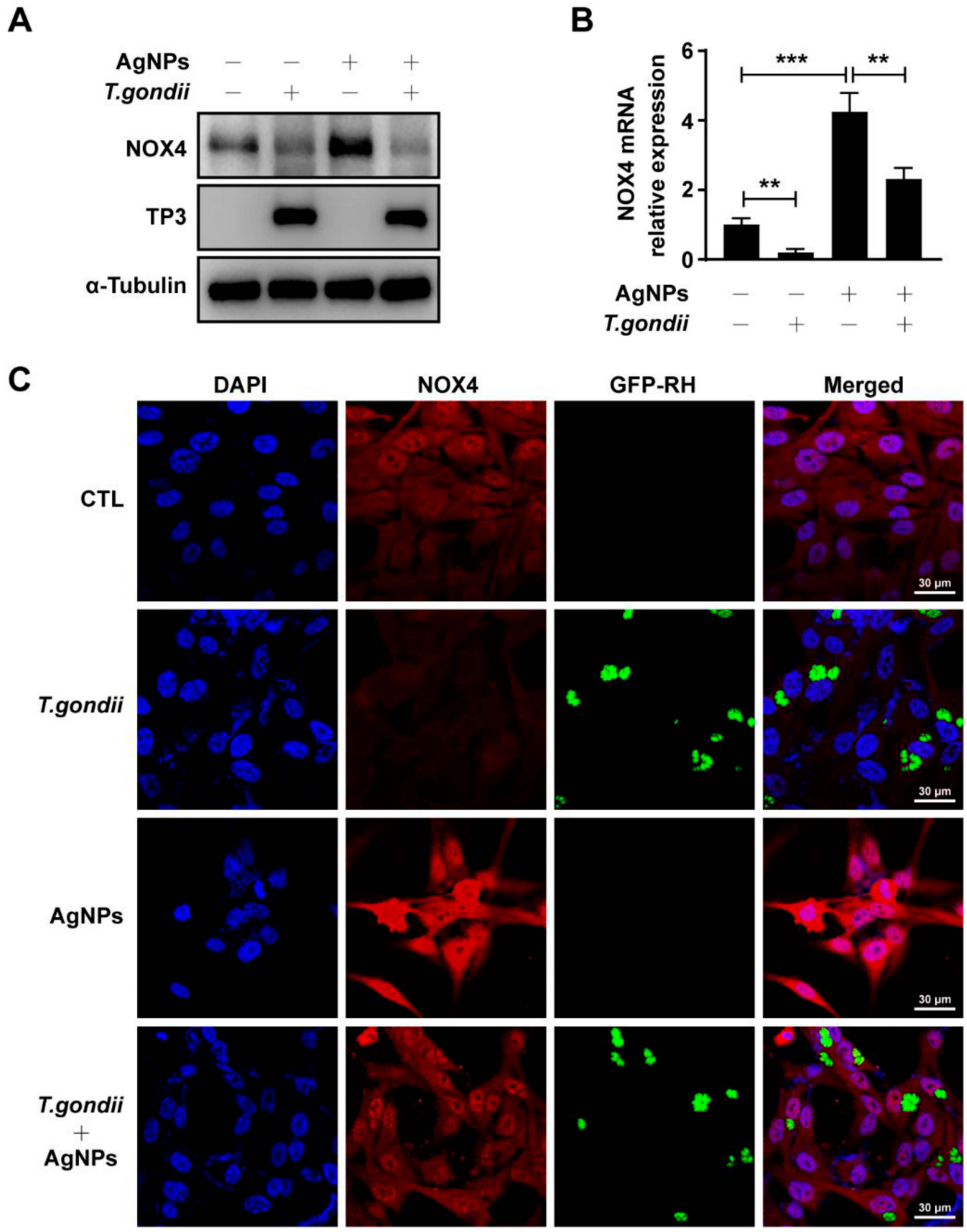

Figure 8 *T. gondii* inhibited AgNP-induced NOX4 production in ARPE-19 cells. Cells were pre-infected with *T. gondii* at MOI 5 for 2 h and treated with or without 5 μg/mL AgNPs for 24 h. (**A**) Protein levels of NOX4 and TP3 were assessed by Western blot analysis. (**B**) NOX4 mRNA levels were determined by qRT-PCR. HPRT1 served as an internal control. (**C**) Cells were stained with NOX4 antibody and detected under a confocal microscope. Representative confocal images of NOX4 expression as red fluorescence. $^{**}P < 0.01$, $^{***}P < 0.001$, as compared to the control group.

Abbreviations: AgNPs, silver nanoparticles; MOI, multiplicity of infection; NOX4, NADPH oxidase 4; TP3, *Toxoplasma gondii* p30 antibody; HPRT1, hypoxanthine phosphoribosyl transferase 1; qRT-PCR, quantitative real-time polymerase chain reaction; DAPI, 4′,6-diamidino-2-phenylindole

treatment, however, cleaved caspase-3-positive cells were significantly decreased after pre-infection with *T. gondii* (Figure 10A). In addition, in wild-type BMDMs, AgNP-treatment dramatically increased cleaved caspase-3-positive cells. In contrast, cleaved caspase-3-positive cells isolated from NOX4 knockout mice BMDMs were significantly decreased (Figure 10B). Similarly, NOX4 protein expression was significantly upregulated upon AgNP treatment in wild-type BMDMs, but this phenomenon was disappeared in BMDMs isolated from NOX4 knockout mice (Figure 10B). Similar results were observed for mitochondrial ROS levels evaluated by MitoSOX red staining. Histograms of the results of FACS analysis showed that in BMDMs isolated from wild-type mice, the percentage of ROS-positive cells was significantly increased in the presence of 5 μg/mL AgNPs for 24 h,

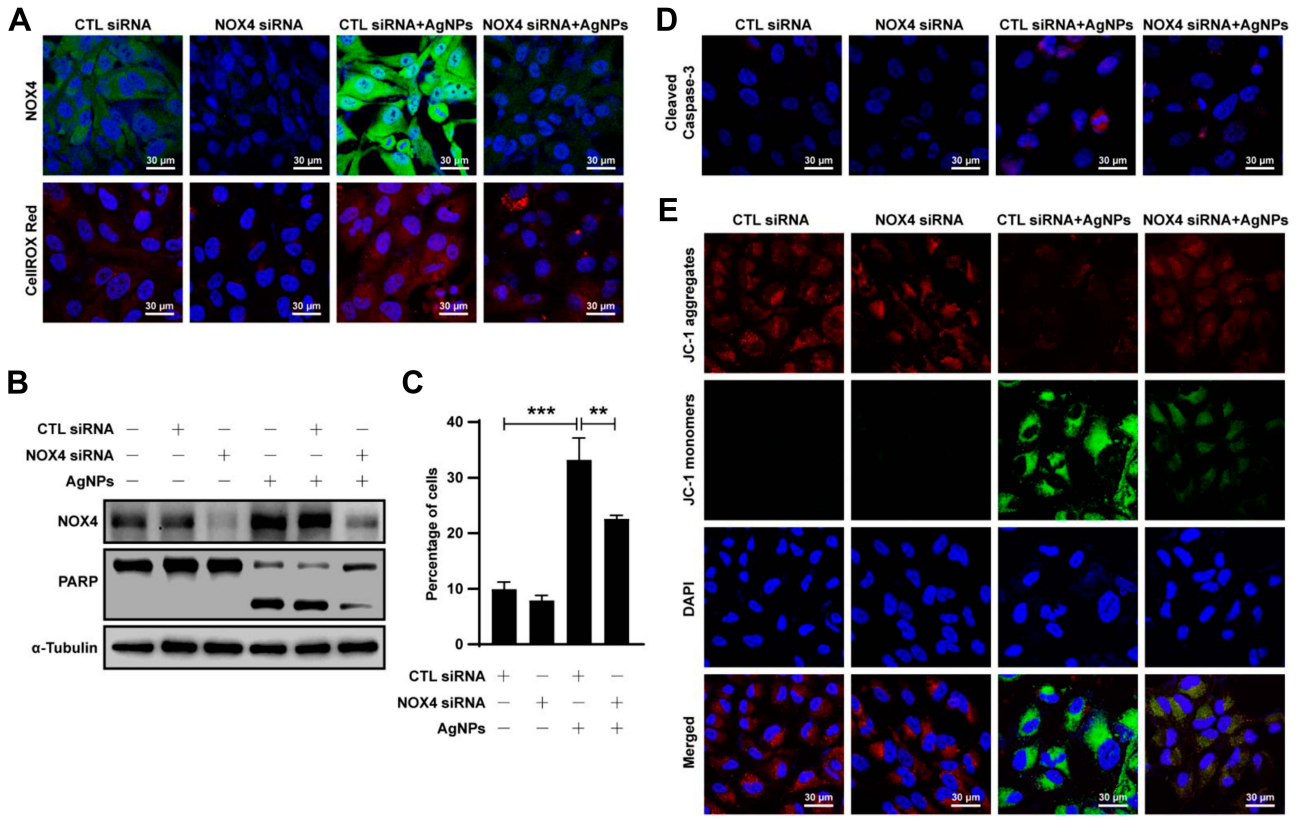

Figure 9 NOX4 gene knockdown suppressed AgNP-induced mitochondrial apoptosis and ROS generation in ARPE-19 cells. ARPE-19 cells were transfected with control siRNA or specific NOX4 siRNAs and treated with 5 μg/mL AgNPs for 24 h. (**A**) Cells were stained with NOX4 (green) antibody or CellROX deep red and detected under a confocal microscope. (**B**) Protein levels of NOX4 and PARP assessed by Western blot analysis. α-Tubulin was used as an internal loading control. (**C**) Mitochondrial ROS levels were measured by flow cytometry after MitoSOX staining. Data are expressed as the mean ± standard deviation of three experiments. $^{**}P < 0.01$, $^{***}P < 0.001$. (**D**) Cleaved caspase-3 was detected by confocal microscopy. (**E**) JC-1 stained cells were observed by confocal imaging. In JC-1 stained cells, red fluorescence is visible in cells with high mitochondrial membrane potential, whereas green fluorescence of JC-1 monomer is present in cells with low mitochondrial potential.

Abbreviations: AgNPs, silver nanoparticles; NOX4, NADPH oxidase 4; siRNA, small interfering RNA; PARP, poly (ADP-ribose) polymerase; ROS, reactive oxygen species; JC-1, 5.5′,6,6′-Tetrachloro-1,1′,3,3′-tetraethyl-imidacarbocyanine iodide; DAPI, 4′,6-diamidino-2-phenylindole

which was significantly inhibited in BMDMs isolated from NOX4 knockout mice (Figure 10C and D). These results strongly suggest that NOX4 was involved in AgNP-induced apoptosis and generation of ROS and that *T. gondii* pre-infection inhibited AgNP-induced apoptosis of BMDM cells by inhibiting the NOX4/ROS pathway.

T. gondii Pre-Infection Prevented AgNP-Induced Mitochondrial Apoptosis by Suppressing NOX4-Dependent ROS Generation in HFF Cells

To further demonstrate the anti-apoptosis effect of *T. gondii* pre-infection through suppression of NOX4-dependent ROS generation, we applied HFF cells. First of all, the HFF cells were treated with various concentrations of AgNPs for 24 h and then apoptotic features were evaluated by Western blotting. As shown in (Figure 11A), AgNPs induced dose-dependent cleavage of caspase-3 and PARP. The cleavage of caspase-3 and PARP became apparent starting at 0.2 μg/mL AgNPs.

Next, to evaluate whether *T. gondii* infection exerts modulatory effects on AgNP-induced apoptosis, HFF cells were first infected with *T. gondii* at MOI 5 for 2 h, and then treated with 5 μg/mL AgNPs for 24 h. Interestingly, Western blotting results indicated that *T. gondii* pre-infection attenuated AgNP-induced cleaves of caspase-3 and PARP protein expressions in HFF cells (Figure 11B). We further evaluated whether *T. gondii*-pretreatment suppressed AgNP-triggered HFF cell apoptosis was mediated by intracellular ROS production, the cells were pre-infected with *T. gondii* at MOI 5 for 2 h and treated with or without 5 μg/mL AgNPs for 24 h. And then evaluated ROS production

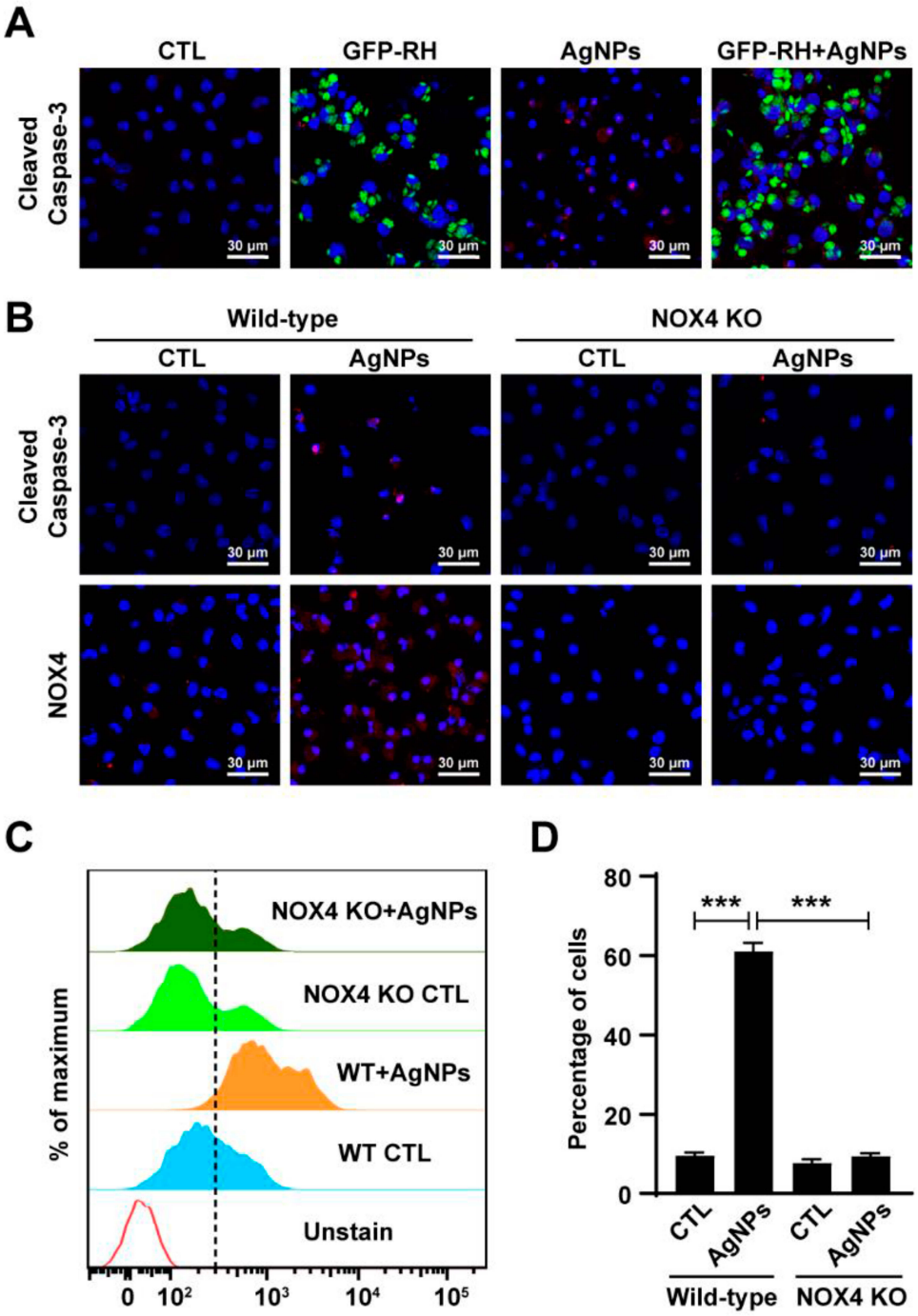

Figure 10 *T. gondii* inhibited AgNP-induced mitochondrial apoptosis and ROS production by suppression of NOX4 expression in murine BMDM cells. (**A**) BMDMs from wild-type mice were infected with GFP-RH (MOI 5) for 2 h and treated with or without 5 μg/mL AgNPs for 24 h. BMDMs were stained with anti-cleaved caspase-3 antibody and detected under a confocal microscope. Representative confocal images of cleaved caspase-3 expression as red fluorescence. (**B**) BMDMs from wild-type or NOX4 knockout mice were treated with or without 5 μg/mL AgNPs for 24 h. BMDMs were stained with anti-cleaved caspase-3 and anti-NOX4 antibody and detected under a confocal microscope. (**C, D**) Mitochondrial ROS levels were measured by flow cytometry after MitoSOX staining. Data are expressed as the mean ± standard deviation of three experiments. ***, $P < 0.001$.

Abbreviations: AgNPs, silver nanoparticles; NOX4, NADPH oxidase 4; BMDMs, bone marrow-derived macrophages; ROS, reactive oxygen species; MOI, multiplicity of infection; ROS, reactive oxygen species

using MitoSOX red mitochondrial superoxide indicator that specifically detects ROS produced within mitochondria. FACS analysis showed that AgNP-treatment significantly increased the percentage of ROS-positive cells, which was reversed by pretreatment with *T. gondii* (Figure 11C).

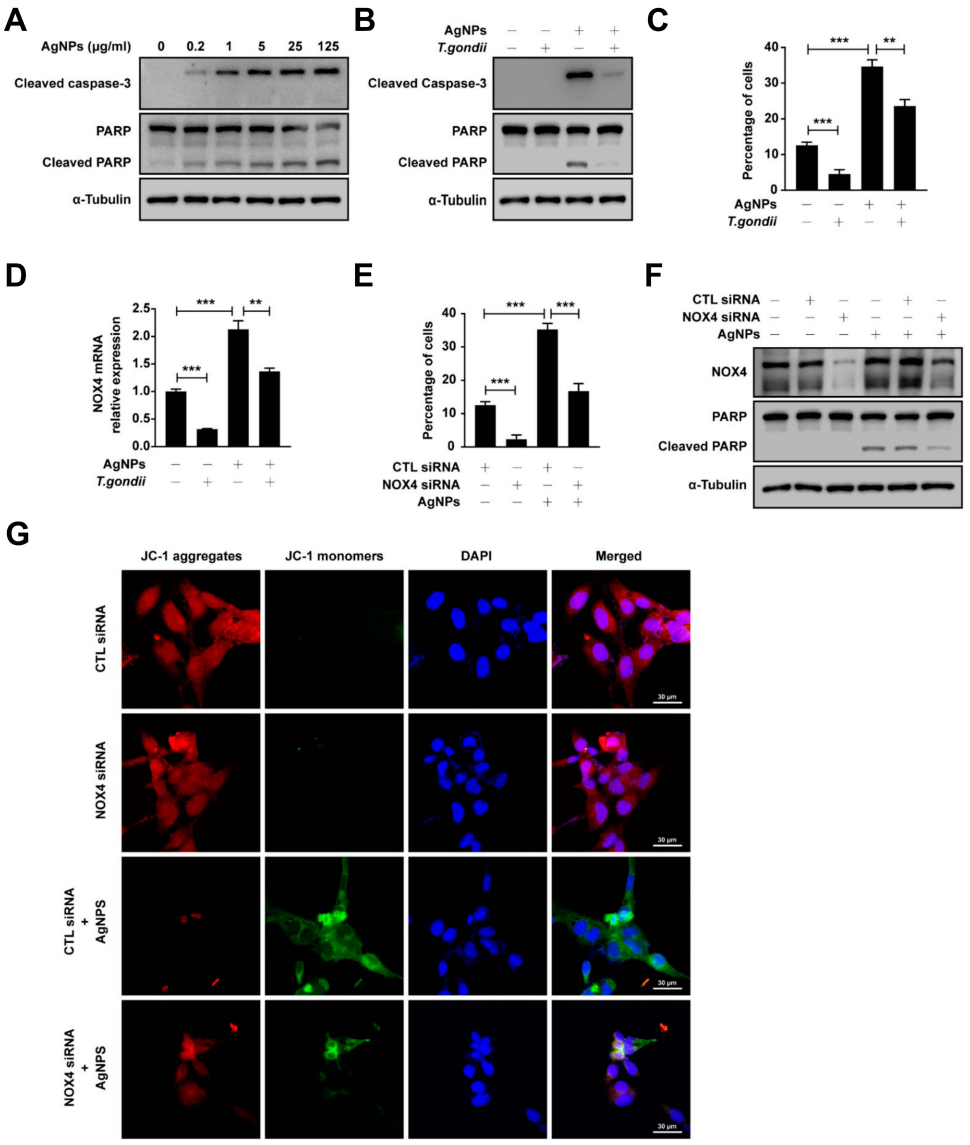

Figure 11 *T. gondii* pre-infection prevented AgNP-induced mitochondrial apoptosis by suppressing NOX4-dependent ROS generation in HFF cells. (**A**) HFF cells were treated with various concentrations of AgNPs for 24 h and protein levels of cleaved caspase-3 and PARP were determined by Western blotting. HFF cells were pre-infected with *T. gondii* at MOI 5 for 2 h and treated with or without 5 μg/mL AgNPs for 24 h. (**B**) The protein levels of cleaved caspase-3 and PARP were determined by Western blotting. (**C**) The cells were loaded with MitoSOX red (5 μM for 30 min) and mitochondrial ROS were detected by flow cytometry. (**D**) NOX4 mRNA levels were determined by qRT-PCR. HPRT1 served as an internal control. HFF cells were transfected with control siRNA or specific NOX4 siRNAs and treated with 5 μg/mL AgNPs for 24 h. (**E**) Mitochondrial ROS levels were measured by flow cytometry after MitoSOX staining. $^{**}P < 0.01$, $^{***}P < 0.001$, as compared to the control or AgNPs-treated group. (**F**) Protein levels of NOX4 and PARP were assessed by Western blot analysis. α-Tubulin was used as an internal loading control. (**G**) JC-1 stained cells were observed by confocal imaging.

Abbreviations: AgNPs, silver nanoparticles; ROS, reactive oxygen species; HFF, human foreskin fibroblast; NOX4, NADPH oxidase 4; PARP, poly (ADP-ribose) polymerase; siRNA, small interfering RNA; JC-1, 5.5′,6,6′-Tetrachloro-1,1′,3,3′-tetraethyl-imidacarbocyanine iodide; DAPI, 4′,6-diamidino-2-phenylindole

To investigate the underlying mechanism of suppression of AgNP-induced mitochondrial ROS by *T. gondii* infection, HFF cells were pre-infected with *T. gondii* at MOI 5 for 2 h and then treated with or without 5 μg/mL AgNPs for 24 h, and then NOX4 expression was evaluated by qRT-PCR. As shown in (Figure 11D), AgNPs significantly increased NOX4 mRNA levels, whereas *T. gondii* pre-infection significantly attenuated AgNP-induced NOX4 mRNA expression. Next, to evaluate the role of NOX4 in AgNP-induced ROS generation, HFF cells which had been incubated for 48 h after transfection with control siRNA or specific NOX4 siRNAs were treated with 5 μg/mL AgNPs for 24 h and then mitochondrial ROS levels were detected. FACS results showed that the percentage of ROS-positive cells was significantly increased for control siRNA-transfected cells in the

presence of 5 μg/mL AgNPs for 24 h, however, dramatically inhibited by NOX4 knockdown (Figure 11E).

Finally, the role of NOX4 in AgNP-induced apoptosis was evaluated by Western blotting analysis and JC-1 staining. The expression levels of NOX4 and cleaved PARP proteins were increased in cells treated with AgNPs, but NOX4 knockdown cells down-regulated the AgNPs-induced expression of cleaved PARP (Figure 11F). Similarly, in control siRNA-transfected cells, AgNPs treatment greatly decreased MMP as evidenced by reduced red and increased green JC-1 fluorescence. However, this phenomenon was reversed by NOX4 siRNA transfection (Figure 11G). In sum, these results clearly indicate that *T. gondii* pre-infection prevented AgNP-induced mitochondrial apoptosis by suppressing NOX4-dependent ROS generation in HFF cells.

Base on the previous study protocol,[27] we prepared the 5% DMSO in medium as a positive control of cell lines. AgNP-induced apoptosis also confirmed again by using 5% DMSO as a positive control in ARPE-19 and HFF cells. Both 5 μg/mL AgNPs and 5% DMSO induced cleaved caspase-3 and PARP protein expression in ARPE-19 and HFF cells. In addition, AgNPs and DMSO induced apoptosis was also evaluated by JC-1 staining. Similarly, AgNPs and DMSO treatment decreased MMP as evidenced by reduced red and increased green JC-1 fluorescence in both ARPE-19 and HFF cells (Supplementary Figure 2).

Discussion

In this study, we found that AgNPs dose-dependently induced cellular toxicity and mitochondrial apoptosis of human RPE ARPE-19 cells. AgNPs treatment also resulted in sub-G1 phase cell accumulation, autophagic cell death, excess ROS production, and JNK activation in ARPE-19 cells; ROS production in AgNP-treated cells was NOX4-dependent. All of these signaling steps relevant to AgNP-induced nanotoxicity were significantly inhibited by *T. gondii* pre-infection in ARPE-19 cells. *T. gondii*-induced inhibition of AgNP-induced mitochondrial apoptosis and NOX4-dependent ROS suppression in ARPE-19 cells was confirmed again in the studies using HFF cells and BMDMs of $NOX4^{-/-}$ mice, suggesting that *T. gondii* strongly inhibits AgNP-induced cytotoxicity through NOX4-dependent ROS suppression.

First, we investigated whether AgNPs induce cytotoxicity of human RPE ARPE-19 cells. In the present study, AgNPs induced the cytotoxicity of ARPE-19 cells in a concentration-dependent manner. We also evaluated the morphological changes of AgNP-treated ARPE-19 cells by assessing the integrity of the microtubule network. After 24 h of AgNP treatment in ARPE-19 cells, we observed condensed chromatin, nucleus fragmentation, and cellular shrinkage of the cells, which are the characteristics of apoptosis.[28] Thus, we further evaluated AgNP-induced apoptosis in ARPE-19 cells more precisely. Apoptosis induction can be activated by two pathways: the extrinsic pathway and the intrinsic (mitochondrial) pathway. In this study, AgNP treatment in ARPE-19 cells increased the levels of Bax, Bik, and Bim proteins, release of cytochrome *c* into the cytosolic fractions of mitochondria, reduction of MMP, and the cleavage of caspase-3 and PARP dose-dependently starting from 0.2 μg/mL AgNPs. These results indicated that AgNP-treated ARPE-19 cells prominently induced mitochondrial apoptosis in a concentration-dependent manner, which agrees with several different reports of cellular toxicity after AgNP exposure.[7–9,29] Polydopamine-coated branched Au–Ag NPs induce an increase in BAX and decrease in Bcl-2 levels, and further provoke depolarization of the MMP and caspase-8 and caspase-3 activation, ultimately causing apoptosis in T24 human bladder cancer cells.[29] Regarding the mechanism of AgNP-induced toxicity, De Matteis et al.[6] described that endocytosed AgNPs are degraded in the lysosomes and the release of Ag^{+} ions in the cytosol induces cell damages, while ions released in the cell culture medium have a negligible effect.

Second, we investigated the mechanisms of AgNP-induced apoptosis in ARPE-19 cells. Several studies have suggested that one of the predominant mechanisms of AgNP-induced toxicity is mediated through oxidative stress in a variety of experimental systems, such as mouse embryonic fibroblasts,[28] vascular endothelial cells,[30] and human liver HepG2 cells.[31] Additionally, AgNPs kill various pathogens and cancer cells such as Candida,[32] Toxoplasma,[33,34] human bladder cancer cells,[29] and hepatoma[31] via the induction of ROS. The results of our study indicated that AgNPs potently and rapidly induce ROS production in ARPE-19 cells, which is similar to the results of other studies.[10,28-32] Next, we further examined the ROS signaling pathway in AgNP-treated ARPE-19 cells. ROS include the superoxide anion, hydrogen peroxide, and hydrogen radical and are generated during mitochondrial oxidative metabolism, as well as in cellular response to xenobiotics, cytokines, and bacterial

invasion.[35] NOX is one of the main sources of ROS production. When NOX is activated, it liberates electrons that bind to oxygen molecules, resulting in the formation of the superoxide anion.[35] In a previous study, we found that NOX4 is the major NOX isoform and an important source of ROS generation in ARPE-19 cells.[26] Thus, we evaluated whether NOX4 is a major source of ROS production in AgNP-treated ARPE-19 cells. In this study, NOX4 was highly expressed in AgNP-treated ARPE-19 cells and was involved in AgNP-induced apoptosis through NOX4-mediated ROS production. Moreover, the inhibition of NOX4 suppressed AgNP-induced mitochondrial apoptosis. These findings are consistent with those of Sun et al.[30] who have reported that AgNPs induce oxidative stress in an NOX4- and Nrf2-dependent manner in vascular endothelial cells.

ROS modulate various cell signaling pathways involved in inflammation, angiogenesis, cell proliferation, and differentiation.[35] In the present study, AgNP treatment increased LC3B levels and the accumulation of cells in the sub-G1 and S phase, especially sub-G1 phase cells. Our findings revealed when ARPE-19 cells are subjected to cytotoxicity by internal or external stimuli, such as NPs, cells fall into autophagic cell death or apoptotic cell death. Previous studies have also reported the induction of autophagy and cell cycle arrest in various cells after treatment with AgNPs.[7,8,28,29] Apoptosis and autophagy are regulated by several signaling pathways, including the AKT/MAPK signaling pathway, in mammalian cells;[36] thus, we examined the involvement of the MAPK signaling pathway. We observed JNK activation in AgNP-treated cells, which is consistent with a previous report, which mentions that AgNPs generate ROS and trigger the JNK pathway, and finally induce mitochondrial apoptosis in NIH3T3 cells.[37] However, Eom et al.[38] have reported that the p38 MAPK signaling pathway is involved in AgNP-induced apoptosis in human Jurkat T cells. Differences in the signaling pathways depend on the study design, such as physico-chemical characterization of NPs, cell types, and treatment conditions.

Third, we evaluated whether *T. gondii* can inhibit the AgNP-induced apoptosis in human ARPE-19 cells. Until now, little is known about the modulators that inhibit the cytotoxicity induced by NPs. Anwar et al.[39] have reported that the toxicity of AgNPs in the liver and kidney of rats significantly decreases after treatment with the herb W. somnifera, which contains free radical scavenging enzymes that function as anti-oxidants. In this study, we selected *T. gondii* as a reducing modulator of nanotoxicity in ARPE-19 cells, as *T. gondii*-mediated resistance to apoptosis has been observed in murine and human cell lines treated with diverse inducers of apoptosis.[17–23] Our study showed that pre-infection of ARPE-19 cells with *T. gondii* inhibited AgNP-induced apoptosis, sub-G1 cell cycle arrest, autophagy, JNK activation by reducing NOX4-mediated ROS production, and finally, apparently abolished AgNP-induced mitochondrial apoptosis in ARPE-19 cells. We also confirmed these results using HFF cells and BMDMs derived from NOX4$^{-/-}$ mice. Our present results indicated that *T. gondii* controls the NOX4-dependent ROS production in ARPE-19 cells to maintain a strong anti-oxidative environment, and then prolongs its parasitism in the cells. However, Adeyemi et al[40] have recently reported that *T. gondii* do not modify cellular apoptosis by inorganic NPs in human fibroblast foreskin cells. The biggest differences between these two studies are the infection time of *T. gondii* into the host cells and the viability of parasites. In this study, the host cells were infected by *T. gondii* 2 h before AgNP treatment; the parasites successfully invaded the host cells and established a favorable environment for multiplying within the infected cells. The cells also resisted various internal and external stimuli using molecules produced from the live *T. gondii* parasites and/or using various systems within the cells.[17–23,41,42] These facts were supported by many other studies mentioning that the inhibitory activity by *T. gondii* requires live intracellular parasites and ongoing protein synthesis.[19–22] However, Adeyemi et al.[40] treated *T. gondii* with various NPs to infect human foreskin fibroblasts and then evaluated apoptosis; thus *T. gondii* may contact NPs immediately and directly and cause damage to invade the host cells.[33,43] Therefore, it would not establish a favorable environment for resisting apoptosis by *T. gondii*. About this one, inorganic NPs kill *T. gondii* by altering the redox status and MMP,[33] and AgNPs induce anti-Toxoplasma potentials by modulating host HIF-1α activity and the tryptophan pathway.[43] In addition, we used a MOI of 5 to infect *T. gondii* into host cells, whereas an MOI of 0.5 was used by Adeyemi et al,[40] which may have affected the amount of ESP produced by the parasites to change the host cell environment. Other differences including the type of host cell and experimental conditions resulted in different results between the two studies.

Regarding the mechanisms of the anti-apoptotic effect by *T. gondii*, Zhou et al.[41] presented that ROP18 of *T. gondii* inhibits ATP-induced host cell apoptosis through

the mitochondrial pathway, regardless of the strain virulence (RH-type I, ME49-type II, and VEG-type III) and host cell lines (human SF268, mouse RAW264.7, and human THP-1 cells). In addition, *T. gondii* can subvert the oxidative stress by activating the parasite's antioxidant network such as peroxiredoxin, glutathione *S*-transferase, glutaredoxin, and thioredoxin reductase of *T. gondii*,[42] and *T. gondii* affects inhibition of the proapoptotic pathway and activation of antiapoptotic pathways in vitro.[22] *T. gondii* also inhibits cytochrome *c*-induced caspase activation in host cells by interfering with holo-apoptosome assembly, and can thus efficiently inhibit the caspase-dependent intrinsic cell death pathway.[23]

In summary, we determined a mechanism of cytotoxicity induced by AgNP in human RPE ARPE-19 cells, and found inhibitory effects of AgNP-induced cytotoxicity in ARPE-19 cells by *T. gondii* pre-infection (Figure 12). This is the first study to evaluate the protection of nanotoxicity using the biological agent *T. gondii*. Further studies are needed to identify other mechanisms of AgNP-induced cytotoxicity in the retina and the molecules in *T. gondii* involved in suppressing AgNP-induced nanotoxicity.

Conclusion

Our study demonstrated that AgNPs induced cytotoxicity in ARPE-19 cells by generating ROS, which was produced mainly through NOX4, JNK phosphorylation, and mitochondria damage, and finally induced mitochondrial apoptosis combined with autophagy and sub-G1 phase cell accumulation. However, *T. gondii* pre-infection protected against the AgNP-induced cytotoxicity of ARPE-19 cells by inhibiting the NOX4/ROS pathways. Although the other mechanisms of AgNP-induced cytotoxicity remain unclear, we suggest one of the mechanisms of cytotoxicity in human RPE ARPE-19 cells by AgNPs, and we found that *T. gondii* is a strong inhibitory modulator of AgNP-induced cytotoxicity in in vitro models.

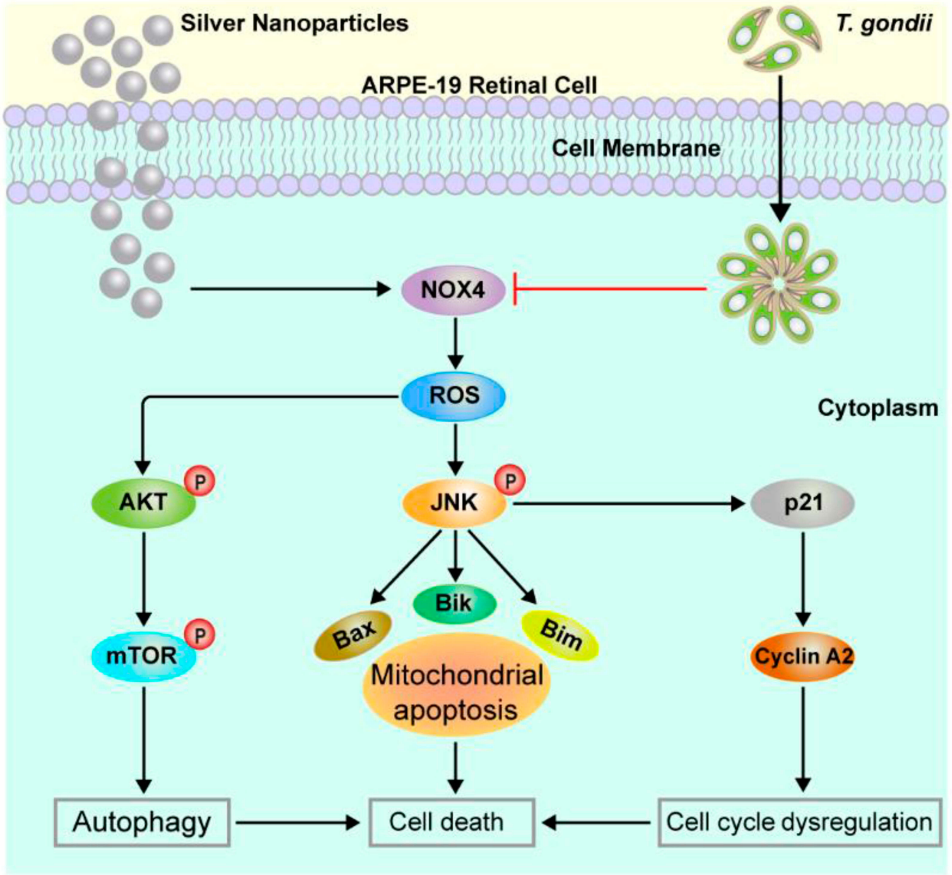

Figure 12 Schematic model of induction of cytotoxicity by AgNPs in ARPE-19 cells, which was inhibited by *T. gondii* pre-infection through inhibition of NOX4-dependent ROS generation.

Abbreviations: AgNPs, silver nanoparticles; NOX4, NADPH oxidase 4; ROS, reactive oxygen species; AKT, protein kinase B; mTOR, mammalian target of rapamycin; JNK, c-Jun N-terminal kinases; Bax, Bcl-2-associated X protein; Bik, BCL2-interacting killer; Bim, Bcl-2-like protein 11; p21, cyclin-dependent kinase inhibitor 1

Ethics and Consent Statement

Animal experimental procedures were approved by the Institutional Animal Care and Use Committee (IACUC) at Chungnam National University (CNU-00706) and conformed to National Institutes of Health guidelines. The animals were fed standard rodent food and water ad libitum and housed (maximum of 5 per cage) in sawdust-lined cages in an air-conditioned environment with 12-h light/dark cycles. Animal husbandry was provided by the staff of the IACUC under the guidance of supervisors who are certified Animal Technologists, and by the staff of the Animal Core Facility. Veterinary care was provided by IACUC faculty members and veterinary residents located on the Chungnam National University College of Medicine.

Data Sharing Statement

The datasets supporting the conclusions of this article are included within the article and its supplementary files. And, the data that support the findings of this study are available from the corresponding author upon reasonable request.

Author Contributions

All authors contributed to experiments, data analysis, drafting and revising the article, gave final approval of the version to be published, and agreed to be accountable for all aspects of the work. In addition, JHQ, FFG, HAHAI and YHL carried out the statistical analyses and organized the data. JMY, GHC and JQC created the figures.

Funding

This work was supported by Basic Science Research Program through the National Research Foundation of Korea (NRF) funded by the Ministry of Science, ICT and Future Planning (NRF-2017R1A2B4012822 and 2019R1A2C1088346) at Chungnam National University, and the National Natural Science Foundation of China (81771612 and 81971389), the Science Foundation of Guangdong Medical University (GDMUZ201801), the Natural Science Foundation of Guangdong Province (2019A1515011888 and 2019A15150 11715). This work was also supported by research fund of Chungnam National University.

Disclosure

The authors declare that the research was conducted in the absence of any commercial or financial relationships that could be construed as a potential conflict of interest.

References

1. Burdușel AC, Gherasim O, Grumezescu AM, Mogoantă L, Ficai A, Andronescu E. Biomedical applications of silver nanoparticles: an up-to-date overview. *Nanomaterials*. 2018;8(9):pii:E681. doi:10.3390/nano8090681
2. Lee SH, Jun BH. Silver nanoparticles: synthesis and application for nanomedicine. *Int J Mol Sci*. 2019;20(4):pii:E865. doi:10.3390/ijms20040865
3. Akter M, Sikder MT, Rahman MM, et al. A systematic review on silver nanoparticles-induced cytotoxicity: physicochemical properties and perspectives. *J Adv Res*. 2017;9:1–16. doi:10.1016/j.jare.2017.10.008
4. Rezvani E, Rafferty A, McGuinness C, Kennedy J. Adverse effects of nanosilver on human health and the environment. *Acta Biomater*. 2019;94:145–159. doi:10.1016/j.actbio.2019.05.042
5. Mohammadinejad R, Moosavi MA, Tavakol S, et al. Necrotic, apoptotic and autophagic cell fates triggered by nanoparticles. *Autophagy*. 2019;15(1):4–33. doi:10.1080/15548627.2018.1509171
6. De Matteis V, Malvindi MA, Galeone A, et al. Negligible particle-specific toxicity mechanism of silver nanoparticles: the role of Ag+ ion release in the cytosol. *Nanomedicine*. 2015;11(3):731–739. doi:10.1016/j.nano.2014.11.002
7. Holmila RJ, Vance SA, King SB, Tsang AW, Singh R, Furdui CM. Silver nanoparticles induce mitochondrial protein oxidation in lung cells impacting cell cycle and proliferation. *Antioxidants*. 2019;8(11):pii:E552. doi:10.3390/antiox8110552
8. Xue Y, Zhang T, Zhang B, Gong F, Huang Y, Tang M. Cytotoxicity and apoptosis induced by silver nanoparticles in human liver HepG2 cells in different dispersion media. *J Appl Toxicol*. 2016;36(3):352–360. doi:10.1002/jat.3199
9. Kalishwaralal K, Banumathi E. Ram Kumar Pandian S, et al. Silver nanoparticles inhibit VEGF induced cell proliferation and migration in bovine retinal endothelial cells. *Colloids Surf B Bioint*. 2009;73(1):51–57. doi:10.1016/j.colsurfb.2009.04.025
10. Söderstjerna E, Bauer P, Cedervall T, et al. Silver and gold nanoparticles exposure to in vitro cultured retina-studies on nanoparticle internalization, apoptosis, oxidative stress, glial- and microglial activity. *PLoS One*. 2014;9(8):e105359. doi:10.1371/journal.pone.0105359
11. Boulton M, Dayhaw-Barker P. The role of the retinal pigment epithelium: topographical variation and ageing changes. *Eye*. 2001;15(Pt 3):384–389. doi:10.1038/eye.2001.141
12. Sheikpranbabu S, Kalishwaralal K, Lee KJ, Vaidyanathan R, Eom SH, Gurunathan S. The inhibition of advanced glycation end-products-induced retinal vascular permeability by silver nanoparticles. *Biomaterials*. 2010;31(8):2260–2271. doi:10.1016/j.biomaterials.2009.11.076
13. Xu L, Li W, Shi Q, et al. Synthesis of mulberry leaf extract mediated gold nanoparticles and their ameliorative effect on aluminium intoxicated and diabetic retinopathy in rats during perinatal life. *J Photochem Photobiol B*. 2019;196:111502. doi:10.1016/j.jphotobiol.2019.04.011
14. Dong Y, Wan G, Yan P, Qian C, Li F, Peng G. Fabrication of resveratrol coated gold nanoparticles and investigation of their effect on diabetic retinopathy in streptozotocin induced diabetic rats. *J Photochem Photobiol B*. 2019;195:51–57. doi:10.1016/j.jphotobiol.2019.04.012
15. Reimondez-Troitiño S, Csaba N, Alonso MJ. de la Fuente M. Nanotherapies for the treatment of ocular diseases. *Eur J Pharm Biopharm*. 2015;95(Pt B):279–293. doi:10.1016/j.ejpb.2015.02.019
16. Weng Y, Liu J, Jin S, Guo W, Liang X, Hu Z. Nanotechnology-based strategies for treatment of ocular disease. *Acta Pharm Sin B*. 2017;7(3):281–291. doi:10.1016/j.apsb.2016.09.001
17. Zhu W, Li J, Pappoe F, Shen J, Yu L. Strategies developed by *Toxoplasma gondii* to survive in the host. *Front Microbiol*. 2019;10:899. doi:10.3389/fmicb.2019.00899

18. Mammari N, Halabi MA, Yaacoub S, Chlala H, Dardé ML, Courtioux B. *Toxoplasma gondii* modulates the host cell responses: an overview of apoptosis pathways. *Biomed Res Int*. 2019;2019:6152489. doi:10.1155/2019/6152489
19. Nash PB, Purner MB, Leon RP, Clarke P, Duke RC, Curiel TJ. *Toxoplasma gondii*-infected cells are resistant to multiple inducers of apoptosis. *J Immunol*. 1998;160(4):1824–1830.
20. Carmen JC, Hardi L, Sinai AP. *T. gondii* inhibits ultraviolet light-induced apoptosis through multiple interactions with the mitochondrion-dependent programmed cell death pathway. *Cell Microbiol*. 2006;8(2):301–315. doi:10.1111/j.1462-5822.2005.00622.x
21. Goebel S, Lüder CG, Gross U. Invasion by *Toxoplasma gondii* protects human-derived HL-60 cells from actinomycin D-induced apoptosis. *Med Microbiol Immunol*. 1999;187(4):221–226. doi:10.1007/s004300050096
22. Quan JH, Cha GH, Zhou W, et al. Involvement of PI 3 kinase/Akt-dependent bad phosphorylation in *toxoplasma gondii*-mediated inhibition of host cell apoptosis. *Exp Parasitol*. 2013;133(4):462–471. doi:10.1016/j.exppara.2013.01.005
23. Graumann K, Schaumburg F, Reubold TF, Hippe D, Eschenburg S, Lüder CG. *Toxoplasma gondii* inhibits cytochrome *c*-induced caspase activation in its host cell by interference with holo-apoptosome assembly. *Microb Cell*. 2015;2(5):150–162. doi:10.15698/mic2015.05.201
24. Jang S, Park JW, Cha HR, et al. Silver nanoparticles modify VEGF signaling pathway and mucus hypersecretion in allergic airway inflammation. *Int J Nanomed*. 2012;7:1329–1343. doi:10.2147/IJN.S27159
25. Kim JH, Lee J, Bae SJ, et al. NADPH oxidase 4 is required for the generation of macrophage migration inhibitory factor and host defense against *Toxoplasma gondii* infection. *Sci Rep*. 2017;7(1):6361. doi:10.1038/s41598-017-06610-4
26. Zhou W, Quan JH, Lee YH, Shin DW, Cha GH. *Toxoplasma gondii* proliferation require down-regulation of host nox4 expression via activation of pi3 kinase/akt signaling pathway. *PLoS One*. 2013;8(6):e66306. doi:10.1371/journal.pone.0066306
27. Kshirsagar P, Sangaru SS, Brunetti V, Malvindi MA, Pompa PP. Synthesis of fluorescent metal nanoparticles in aqueous solution by photochemical reduction. *Nanotechnology*. 2014;25(4):045601. doi:10.1088/0957-4484/25/4/045601
28. Lee YH, Cheng FY, Chiu HW, et al. Cytotoxicity, oxidative stress, apoptosis and the autophagic effects of silver nanoparticles in mouse embryonic fibroblasts. *Biomaterials*. 2014;35(16):4706–4715. doi:10.1016/j.biomaterials.2014.02.021
29. Zhao X, Qi T, Kong C, et al. Photothermal exposure of polydopamine-coated branched Au-Ag nanoparticles induces cell cycle arrest, apoptosis, and autophagy in human bladder cancer cells. *Int J Nanomed*. 2018;13:6413–6428. doi:10.2147/IJN.S174349
30. Sun X, Yang Y, Shi J, Wang C, Yu Z, Zhang H. NOX4- and Nrf2-mediated oxidative stress induced by silver nanoparticles in vascular endothelial cells. *J Appl Toxicol*. 2017;37(12):1428–1437. doi:10.1002/jat.3511
31. Zhu B, Li Y, Lin Z, et al. Silver nanoparticles induce HePG-2 cells apoptosis through ros-mediated signaling pathways. *Nanoscale Res Lett*. 2016;11(1):198. doi:10.1186/s11671-016-1419-4
32. Jalal M, Ansari MA, Alzohairy MA, et al. Anticandidal activity of biosynthesized silver nanoparticles: effect on growth, cell morphology, and key virulence attributes of *Candida* species. *Int J Nanomed*. 2019;14:4667–4679. doi:10.2147/IJN.S210449
33. Adeyemi OS, Murata Y, Sugi T, Kato K. Inorganic nanoparticles kill *Toxoplasma gondii* via changes in redox status and mitochondrial membrane potential. *Int J Nanomed*. 2017;12:1647–1661. doi:10.2147/IJN.S122178
34. Teimouri A, Azami SJ, Keshavarz H, et al. Anti-*toxoplasma* activity of various molecular weights and concentrations of chitosan nanoparticles on tachyzoites of RH strain. *Int J Nanomed*. 2018;13:1341–1351. doi:10.2147/IJN.S158736
35. Bedard K, Krause KH. The NOX family of ROS-generating NADPH oxidases: physiology and pathophysiology. *Physiol Rev*. 2007;87(1):245–313. doi:10.1152/physrev.00044.2005
36. Zhao GX, Pan H, Ouyang DY, He XH. The critical molecular interconnections in regulating apoptosis and autophagy. *Ann Med*. 2015;47(4):305–315. doi:10.3109/07853890.2015.1040831
37. Hsin YH, Chen CF, Huang S, Shih TS, Lai PS, Chueh PJ. The apoptotic effect of nanosilver is mediated by a ROS- and JNK-dependent mechanism involving the mitochondrial pathway in NIH3T3 cells. *Toxicol Lett*. 2008;179(3):130–139. doi:10.1016/j.toxlet.2008.04.015
38. Eom HJ, Choi J. p38 MAPK activation, DNA damage, cell cycle arrest and apoptosis as mechanisms of toxicity of silver nanoparticles in Jurkat T cells. *Environ Sci Technol*. 2010;44(21):8337–8342. doi:10.1021/es1020668
39. Anwar MF, Yadav D, Rastogi S, et al. Modulation of liver and kidney toxicity by herb *Withania somnifera* for silver nanoparticles: a novel approach for harmonizing between safety and use of nanoparticles. *Protoplasma*. 2015;252(2):547–558. doi:10.1007/s00709-014-0701-5
40. Adeyemi OS, Otohinoyi DA, Awakan OJ, Adeyanju AA. Cellular apoptosis of HFF cells by inorganic nanoparticles not susceptible to modulation by *Toxoplasma gondii* infection in vitro. *Toxicol in Vitro*. 2019;54:280–285. doi:10.1016/j.tiv.2018.10.011
41. Zhou LJ, Chen M, Puthiyakunnon S, et al. *Toxoplasma gondii* ROP18 inhibits human glioblastoma cell apoptosis through a mitochondrial pathway by targeting host cell P2X1. *Parasit Vectors*. 2019;12(1):284. doi:10.1186/s13071-019-3529-1
42. Ding M, Kwok LY, Schlüter D, Clayton C, Soldati D. The antioxidant systems in *Toxoplasma gondii* and the role of cytosolic catalase in defence against oxidative injury. *Mol Microbiol*. 2004;51(1):47–61.
43. Adeyemi OS, Murata Y, Sugi T, Han Y, Kato K. Modulation of host HIF-1α activity and the tryptophan pathway contributes to the anti-*Toxoplasma gondii* potential of nanoparticles. *Biochem Biophys Rep*. 2017;11:84–92. doi:10.1016/j.bbrep.2017.07.004